A&A 379, 634–659 (2001)
DOI: 10.1051/0004-6361:20011330

Astronomy & Astrophysics

Stellar encounters with the solar system

J. García-Sánchez[1], P. R. Weissman[2], R. A. Preston[2], D. L. Jones[2], J.-F. Lestrade[3], D. W. Latham[4], R. P. Stefanik[4], and J. M. Paredes[1]

[1] Departament d'Astronomia i Meteorologia, Universitat de Barcelona, Av. Diagonal 647, 08028 Barcelona, Spain
[2] Jet Propulsion Laboratory, California Institute of Technology, 4800 Oak Grove Drive, Pasadena, CA 91109, USA
[3] Observatoire de Paris/DEMIRM-CNRS8540, 77 Av. Denfert Rochereau, 75014 Paris, France
[4] Harvard-Smithsonian Center for Astrophysics, 60 Garden Street, Cambridge, MA 02138, USA

Received 20 April 2001 / Accepted 17 September 2001

Abstract. We continue our search, based on Hipparcos data, for stars which have encountered or will encounter the solar system (García-Sánchez et al. 1999). Hipparcos parallax and proper motion data are combined with ground-based radial velocity measurements to obtain the trajectories of stars relative to the solar system. We have integrated all trajectories using three different models of the galactic potential: a local potential model, a global potential model, and a perturbative potential model. The agreement between the models is generally very good. The time period over which our search for close passages is valid is about ±10 Myr. Based on the Hipparcos data, we find a frequency of stellar encounters within one parsec of the Sun of 2.3 ± 0.2 per Myr. However, we also find that the Hipparcos data is observationally incomplete. By comparing the Hipparcos observations with the stellar luminosity function for star systems within 50 pc of the Sun, we estimate that only about one-fifth of the stars or star systems were detected by Hipparcos. Correcting for this incompleteness, we obtain a value of 11.7 ± 1.3 stellar encounters per Myr within one pc of the Sun. We examine the ability of two future missions, FAME and GAIA, to extend the search for past and future stellar encounters with the Sun.

Key words. comets: general – stars: general – stars: kinematics – Galaxy: general

1. Introduction

Comets in the Oort cloud evolve dynamically under the influence of external perturbers. Their orbits are perturbed by random passing stars, by giant molecular clouds, and by the galactic gravitational field. In particular, the random motions of the stars and the Sun occasionally bring a star very close to the Sun. Close or penetrating passages through the Oort cloud can deflect large numbers of comets on to orbits that enter the planetary region (Hills 1981; Weissman 1996), thus triggering what are known as comet showers. Some terrestial impact craters and stratigraphic records of impact and extinction events on Earth (Hut et al. 1987), as well as geochemical evidence (Farley et al. 1998), suggest that such showers may have occurred in the past. The determination of the frequency of stellar encounters with the Sun is the starting point in the investigation of the role played by external perturbers, over the history of the solar system, on the dynamical evolution of the population of Oort cloud comets. Therefore, it is important for our understanding of the solar system to answer questions such as how close and how often stellar encounters with the solar system occur, and what are the consequences for the dynamics of the cometary cloud.

The limited accuracy of pre-Hipparcos astrometric data, that is ground-based parallax and proper motion measurements, imposed a severe limitation on the accuracy of predictions of past or future close stellar passages. A significant improvement in the accuracy of astrometric data was achieved by the Hipparcos mission (ESA 1997). For instance, Jahreiss & Wielen (1997) compared the best available ground-based trigonometric parallaxes of 1452 star systems with Hipparcos parallax values of the same systems. They found that the median standard error of the Hipparcos parallaxes is 1.15 milliarcsec (mas) compared to 8.8 mas for the best ground-based parallaxes, and that 40% of the ground-based parallaxes have errors exceeding 10 mas, compared with only 2% of the Hipparcos parallaxes. According to Hipparcos measurements, only 66% of the stars with ground-based distances closer than 25 pc are really within 25 pc. Using Hipparcos data, much better answers to the questions above can be obtained.

Send offprint requests to: J. García-Sánchez
e-mail: joan.garcia@tin.it

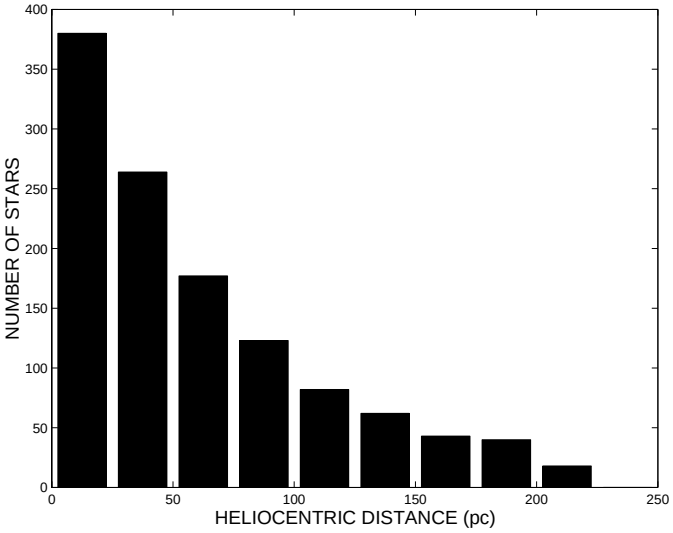

Fig. 1. Number of Hipparcos stars in our sample in each 25 pc bin as a function of distance from the Sun.

In García-Sánchez et al. (1997) we began the search for stars passing close to the Sun using Hipparcos data, assuming a simple linear motion model. In García-Sánchez et al. (1999, hereafter Paper I) we continued this search by integrating the motion of the candidate stars and the Sun in the local galactic potential. Based on radial velocity measurements from the literature as well as others from our own observations, we identified a few passing stars whose encounters with the solar system could potentially cause a perturbation of the Oort cloud. We performed dynamical simulations of cometary orbits using a Monte Carlo model to estimate if there is a significant increase in the long-period comet flux at the Earth's orbit caused by these potential perturbers. The strongest perturbation is for the future encounter with GL 710, though no substantial enhancement of the steady-state cometary flux would result from this passage.

In the present paper, we extend our search for close passages to more candidate stars by using new measurements of radial velocities, as well as considering several analytical expressions of the potential of the Galaxy to integrate the equations of motion. We study the limits of validity of our results, and how these limits may be expanded by new astrometric data from future space-based astrometric missions. In addition, we estimate the frequency of encounters with the Sun from the identified encounters taking into account the observational incompleteness of the Hipparcos data.

In Sect. 2 we present the data sources and the selection criteria for candidate stars used in the search for stellar encounters. In Sect. 3 we describe the equations of motion and the potential models of the Galaxy that will be used to compute the stellar galactic orbits. In Sect. 4 we discuss the range of values of the galactic parameters to be taken into account in the potential models, as well as the choice of the potential model that is the best suited to our study. The results of the predicted encounters with the solar system are presented in Sect. 5. In Sect. 6 we analyze different sources of uncertainty that may constrain this study and the valid time interval for agreement between potential models. In Sect. 7 we determine the frequency of encounters with the Sun using different methods. In Sect. 8 we asses the future impact of two space-based astrometric missions, GAIA and FAME. Finally, our conclusions are given in Sect. 9.

2. The candidate stars

Our astrometric data set consists of the right ascensions, α, declinations, δ, trigonometric parallaxes, π, and the proper motion components in right ascension, $\mu_{\alpha\star} = \mu_\alpha \cos\delta$, and declination, μ_δ, of the stars contained in the Hipparcos Catalogue.

As in Paper I, in order to construct a sample of candidate stars that could have or could have had a passage close to the solar system, we selected stars from the Hipparcos Catalogue whose proper motion, combined with an assumed maximum velocity of 100 $\mathrm{km\,s^{-1}}$, implied an impact parameter (closest approach distance) of 3 pc or less. This velocity limit is several times the local stellar velocity dispersion, so that intrinsically high velocity stars are included. At that velocity this requirement means that stars whose proper motion in mas/yr is less than 0.06 times the square of the parallax in mas, are the best candidates to have approaches within 3 pc from the Sun. We selected stars with parallax values greater than 4.5 mas because for smaller values the implied proper motion limit would be close to or below the Hipparcos measurement accuracy.

The impact parameter of 3 pc allows inclusion of relatively distant passages of massive stars or star systems that might affect the cometary orbits. The net heliocentric velocity impulse gained by an Oort cloud comet as a result of a stellar passage is proportional to $M_* v_*^{-1} D_{\mathrm{ca}}^{-2}$ (Rickman 1976), where M_*, v_* and D_{ca} are the mass, encounter velocity and closest approach distance, respectively, of the passing star or star system. Very close passages are expected to be the most likely to significantly perturb the Oort cloud. However, perturbations could also be possible for somewhat more distant ones, depending on how long the encounter lasts and how massive the stars or multiple star systems encountered are.

According to the above criteria, and after elimination of a few stars with unreliable astrometric values, we found a total of 1189 candidates that satisfied our search criteria. The distribution of the candidate stars with distance is shown in Fig. 1. The number of sample stars decreases with distance, with 80% of the stars within a heliocentric distance of 100 pc, and only 20% between 100 and 225 pc.

We searched the literature for published radial velocity measurements for the selected stars. We also made radial velocity measurements using the Center for Astrophysics (CfA) digital speedometers (Latham 1985, 1992) for some of the stars, as part of an observational program to measure radial velocities of candidate stars with no previous

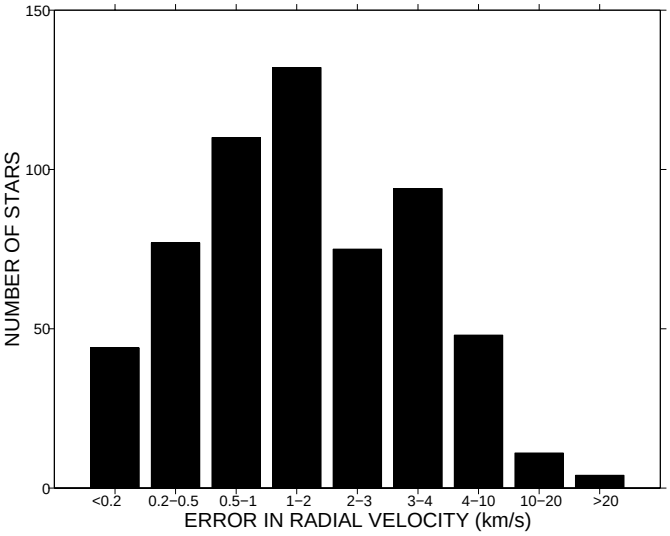

Fig. 2. Distribution of the radial velocity errors for the 595 candidate stars with measurements. Note that different bin widths are used.

measurements (see Paper I for details). We found values for a total of 595 of the 1189 candidate stars, 518 in the literature plus 77 observed at the CfA, about 50% of the total number selected. We plot the distribution of errors in the radial velocities of these 595 stars in Fig. 2.

3. Potential models

In order to determine the stellar encounters with the solar system, we consider the three-dimensional Newtonian equations of motion of a star with respect to the galactic center to compute the stellar trajectories under the galactic gravitational forces. Assuming a steady-state Galaxy with gravitational potential Φ, these equations can be expressed in cylindrical coordinates (R, θ, z) centered on the galactic nucleus as (Mihalas & Routly 1968)

$$\ddot{R} - R\dot{\theta}^2 = -\frac{\partial \Phi}{\partial R} \quad (1)$$

$$R^2\ddot{\theta} + 2R\dot{R}\dot{\theta} = -\frac{\partial \Phi}{\partial \theta} \quad (2)$$

$$\ddot{z} = -\frac{\partial \Phi}{\partial z}. \quad (3)$$

We will consider three models of the galactic potential that can be introduced in the equations of motion above. The first is a simple local potential model, which is based on the observed local features in the solar neighborhood. The second is the global potential model, and takes into account the large scale features of the Galaxy. Both the local and the global galactic potential models adopt an axisymmetric galactic potential, which implies that the partial derivatives of this potential with respect to θ are zero. This axisymmetry is broken when we consider the third model, the global model with the added perturbative contribution of the spiral arms of the Galaxy.

3.1. Local potential model

We assume that for stars not far from the galactic plane (small values of z/R), the galactic force can be expressed in terms of two components: a radial force K_R that governs the motion in the galactic plane, and a vertical force K_z that depends on the local mass density. Expanding the galactic force field in the plane to first order around the Sun's galactocentric distance $R_\odot$, the following empirical expression for the radial force K_R (e.g., Trumpler & Weaver 1953) can be derived:

$$K_R \simeq K_{R_\odot} + \left(\frac{\mathrm{d}K_R}{\mathrm{d}R}\right)_\odot (R - R_\odot). \quad (4)$$

Introducing $K_R = -\partial\Phi/\partial R$, the corresponding potential expression can be derived:

$$\frac{\partial \Phi}{\partial R} \simeq \left(\frac{\partial \Phi}{\partial R}\right)_\odot + \left[\frac{\mathrm{d}}{\mathrm{d}R}\left(\frac{\partial \Phi}{\partial R}\right)\right]_\odot (R - R_\odot). \quad (5)$$

Introducing the expressions

$$\left(\frac{\partial \Phi}{\partial R}\right)_\odot = \frac{\Theta_\odot^2}{R_\odot} \quad (6)$$

and

$$\left[\frac{\mathrm{d}}{\mathrm{d}R}\left(\frac{\partial \Phi}{\partial R}\right)\right]_\odot = 2\frac{\Theta_\odot}{R_\odot}\left(\frac{\mathrm{d}\Theta}{\mathrm{d}R}\right)_\odot - \frac{\Theta_\odot^2}{R_\odot^2} \quad (7)$$

into Eq. (5), with $\Theta_\odot = \Omega_\odot R_\odot$ being the circular velocity at the Sun's position, we obtain

$$\frac{\partial \Phi}{\partial R} = \Omega_\odot^2 R_\odot + \left(2\Omega_\odot\left(\frac{\mathrm{d}\Theta}{\mathrm{d}R}\right)_\odot - \Omega_\odot^2\right)(R - R_\odot). \quad (8)$$

For the perpendicular motion relative to the galactic plane, we can use Poisson's equation to derive $\partial\Phi/\partial z$. Poisson's equation, to first order, is

$$4\pi G\rho_\odot = -\frac{\partial K_z}{\partial z} \quad (9)$$

where $\rho_\odot$ is the mass density in the solar neighborhood. The term neglected in this equation, $2(A^2 - B^2)$, where A and B are the Oort constants, is zero for a flat galactic rotation curve and small for other rotation curves. Since $K_z = -\partial\Phi/\partial z$, we can write:

$$\frac{\partial \Phi}{\partial z} = 4\pi G\rho_\odot z. \quad (10)$$

3.2. Global potential model

Next we move to a more global view of the Galaxy, and consider a galactic mass model based on the large scale features of the Galaxy. The structure of the Galaxy can be modeled as the contributions of three components – a bulge, a disk and a halo – in order to reproduce the global galactic gravitational potential.

In the present case, the total axisymmetric galactic potential can be expressed as the sum of the contributions of each component:

$$\Phi \equiv \Phi_{\rm gl} = \Phi_{\rm b} + \Phi_{\rm d} + \Phi_{\rm h} \tag{11}$$

where $\Phi_{\rm b}$, $\Phi_{\rm d}$ and $\Phi_{\rm h}$ are the potentials generated by the bulge, disk and halo, respectively.

For the potential-density pair of the spherically symmetric bulge and halo components, we adopt Plummer's (1911) model which can be written as

$$\Phi_{\rm b,h} = -\frac{GM_{\rm b,h}}{\sqrt{R^2 + z^2 + b_{\rm b,h}^2}} \tag{12}$$

whereas for the axisymmetric disk we adopt the Miyamoto & Nagai (1975) form of Kuzmin's (1956) model:

$$\Phi_{\rm d} = -\frac{GM_{\rm d}}{\sqrt{R^2 + \left(a_{\rm d} + \sqrt{z^2 + b_{\rm d}^2}\right)^2}}. \tag{13}$$

In the above expressions $M_{\rm b}$, $M_{\rm d}$ and $M_{\rm h}$ are the mass of the bulge, disk and halo, respectively, $a_{\rm d}$ is the scale length of the disk, and $b_{\rm b}$, $b_{\rm d}$ and $b_{\rm h}$ are the scale heights of the bulge, disk and halo, respectively.

3.3. Perturbative potential model

We next consider the effect of a small-amplitude density perturbation of the galactic potential, such as the perturbing spiral gravitational potential superimposed on the axisymmetric galactic disk by the existence of spiral arms. We assume that the spiral arms are a rigidly rotating pattern on the galactic disk that sets up a local minimum in the gravitational field of the disk.

The potential $\Phi_{\rm s}$ associated with this perturbation can in general be described as a superposition of elementary waves of the form (see, e.g., Yuan 1969a,b; Bertin & Lin 1996):

$$\Phi_{\rm s} = \Re{\rm e}\{\Upsilon(R){\rm e}^{i(\omega t - m\theta)}\} \tag{14}$$

where m is the number of spiral arms. The parameter ω is related to the angular speed at which the spiral pattern rotates about the galactic center, $\Omega_{\rm p}$, through $\omega = m\ \Omega_{\rm p}$. The function $\Upsilon(R)$ is

$$\Upsilon(R) = A(R){\rm e}^{i\Psi(R)} \tag{15}$$

where $A(R)$ is the amplitude and $\Psi(R)$ is the phase term. The amplitude $A(R)$ is a slowly varying function of R, and for our purposes is taken to be

$$A = \frac{FR_\odot^2\Omega_\odot^2 \tan\gamma}{m} \tag{16}$$

with F being the ratio of the radial component of the spiral field to the symmetrical field, and γ the pitch angle of the spiral arm given by

$$\tan\gamma = \frac{m}{2\pi} \ln\left(1 + \frac{\Delta R}{R_{\rm a}}\right). \tag{17}$$

In the expression above, $R_{\rm a}$ is the location of the center of the spiral arm in the direction of the galactic center and ΔR is the separation between arms. The phase term $\Psi(R)$ is

$$\Psi(R) = \Psi_\odot - \frac{m}{\tan\gamma} \ln\left(\frac{R}{R_\odot}\right) \tag{18}$$

where $\Psi_\odot$ is a constant that can be determined from the condition of minimum of the potential (that is, for $t = 0$, $\theta = 0^{\rm o}$, $\Psi(R) = \pi$).

Following Yuan (1969b), we can express Eq. (14) as

$$\Phi_{\rm s} = A\cos\left(m\left(\Omega_{\rm p}t - \theta\right) + \Psi(R)\right). \tag{19}$$

To obtain the total potential Φ used in the equations of motion, $\Phi_{\rm s}$ is added to the axisymmetric global potential, denoted as $\Phi_{\rm gl}$ and given by (11). Thus, the total potential is given as

$$\Phi = \Phi_{\rm gl} + \Phi_{\rm s} \tag{20}$$

where the partial derivatives with respect to R, θ and z are

$$\frac{\partial\Phi}{\partial R} = \frac{\partial\Phi_{\rm gl}}{\partial R} + \frac{\partial\Phi_{\rm s}}{\partial R} \tag{21}$$

$$\frac{\partial\Phi}{\partial\theta} = \frac{\partial\Phi_{\rm gl}}{\partial\theta} + \frac{\partial\Phi_{\rm s}}{\partial\theta} = \frac{\partial\Phi_{\rm s}}{\partial\theta} \tag{22}$$

$$\frac{\partial\Phi}{\partial z} = \frac{\partial\Phi_{\rm gl}}{\partial z} + \frac{\partial\Phi_{\rm s}}{\partial z} = \frac{\partial\Phi_{\rm gl}}{\partial z}. \tag{23}$$

4. Galactic parameters and choice of potential model

We discuss here the values of the parameters to be used in the equations of motion described above. Our aim is to construct a set of plausible and self-consistent values of the galactic parameters, according to observational constraints in the literature, from which the stellar passages can then be determined.

4.1. Solar and galactic parameters in the local potential model

For the Sun's velocity with respect to the Local Standard of Rest (LSR), we adopt the values of 9.3 ± 0.8 km s^{-1} in the direction of the galactic center, 11.2 ± 0.7 km s^{-1} in the direction of galactic rotation, and 7.6 ± 0.6 km s^{-1} towards the north galactic pole, as reported by Feast & Whitelock (1997), and very similar to Delhaye's (1965) classical values of (9, 12, 7) km s^{-1}. An accurate value for the Sun's vertical height above the plane, $z_\odot$, is not well established. Past studies report values of $z_\odot$ ranging from about 10 to 42 pc, depending on the method used (see Humphreys & Larsen 1995 for a review). Reed (1997) estimated that $z_\odot$ is likely not less than ∼6 pc and no more than ∼13 pc above the galactic midplane based on OB star counts. Hipparcos studies also report low heights, $z_\odot \simeq 8 \pm 4$ pc according to Holmberg et al. (1997)

Table 1. Values of the solar and galactic parameters adopted.

Sun's motion	(9.3, 11.2, 7.6) km s^{-1}
Sun's height	$z_\odot = 10$ pc
Galactocentric distance	$R_\odot = 7.5$–8.5 kpc
Local mass density	$\rho_\odot = 0.076$–0.15 $M_\odot$ pc^{-3}
Local angular velocity	$\Omega_\odot = 27.19$ km s^{-1} kpc^{-1}
	$(\mathrm{d}\Theta/\mathrm{d}R)_\odot = -2.4$ km s^{-1} kpc^{-1}
Rotation constants	$A = 14.82$ km s^{-1} kpc^{-1}
	$B = -12.37$ km s^{-1} kpc^{-1}

and $z_\odot = 9 \pm 4$ pc according to Pham (1997). We adopt a rounded-off value of $z_\odot = 10$ pc. We will show later that the use of other plausible values of $z_\odot$ does not significantly affect our calculations. The IAU standard value for the Sun's galactocentric distance is $R_\odot = 8.5 \pm 1.1$ kpc (Kerr & Lynden-Bell 1986). However, more recent studies show a trend towards smaller values of $R_\odot$. Reid (1993) examined this question and found a best value of $R_\odot = 8.0 \pm 0.5$ kpc. Feast & Whitelock (1997), in a study of the local galactic kinematics based on Hipparcos proper motion measurements of Cepheids, derived $R_\odot = 8.5 \pm 0.5$ kpc. In constrast, Olling & Merrifield (1998) also studied the rotation curve of the Galaxy and derived $R_\odot = 7.1 \pm 0.5$ kpc, a value that they claim to be consistent with the kinematic study by Feast & Whitelock (1997). In our study we adopt the range $R_\odot = 7.5$–8.5 kpc as the most reliable values.

By "galactic parameters", we refer here to those that characterize the amount of matter and the rotation of the Galaxy in the solar neighborhood. Several studies have been carried out to determine the local mass density $\rho_\odot$ dynamically, leading to conflicting results. Whereas some authors claimed the presence of disk dark matter greater than 50% of the observed matter (Bahcall 1984a,b; Bahcall et al. 1992), others estimated a much lower value or even zero disk dark matter (Bienaymé et al. 1987; Kuijken & Gilmore 1989). Work based on Hipparcos data seems to support a low value of the local dynamical mass density; Crézé et al. (1998) found $\rho_\odot = 0.076 \pm 0.015$ $M_\odot$ pc^{-3}, Holmberg & Flynn (2000) found $\rho_\odot = 0.102 \pm 0.01$ $M_\odot$ pc^{-3}, and Pham (1997) found $\rho_\odot = 0.11 \pm 0.01$ $M_\odot$ pc^{-3}. The differences in the Hipparcos results are mainly due to the methods applied. We adopt the range $\rho_\odot = 0.076$–0.15 $M_\odot$ pc^{-3} in our study.

Based on Hipparcos proper motions of Cepheids, Feast & Whitelock (1997) derived Oort constants of $A = 14.82 \pm 0.84$ km s^{-1} kpc^{-1} and $B = -12.37 \pm 0.64$ km s^{-1} kpc^{-1}. These results are essentially independent of the value of $R_\odot$ used. Feast & Whitelock also derived an angular velocity of circular rotation of $\Omega_\odot = 27.19 \pm 0.87$ km s^{-1} kpc^{-1}, in very good agreement with the value of 27.2 ± 1.7 km s^{-1} kpc^{-1} derived by Reid et al. (1999), and a slowly declining galactic rotation curve at $R_\odot$, given by $(\mathrm{d}\Theta/\mathrm{d}R)_\odot = -2.4 \pm 1.2$ km s^{-1} kpc^{-1}. We adopt these values in our calculations.

Table 2. Adopted constants $R_\odot$ and $\Theta_\odot$, model constants and computed local parameters of the model of Dauphole & Colin (1995).

Sun's Galactocentric dist.	$R_\odot = 8.0$ kpc
Local circular velocity	$\Theta_\odot = 225$ km s^{-1}
Local angular velocity	$\Omega_\odot = 28.125$ km s^{-1} kpc^{-1}
Bulge constants	$M_\mathrm{b} = 1.3955\times10^{10}$ $M_\odot$
	$b_\mathrm{b} = 0.35$ kpc
Disk constants	$M_\mathrm{d} = 7.9080\times10^{10}$ $M_\odot$
	$a_\mathrm{d} = 3.55$ kpc
	$b_\mathrm{d} = 0.25$ kpc
Halo constants	$M_\mathrm{h} = 6.9766\times10^{11}$ $M_\odot$
	$b_\mathrm{h} = 24.0$ kpc
Local mass density	$\rho_\odot = 0.143$ $M_\odot$ pc^{-3}
Rotation constants	$A = 14.25$ km s^{-1} kpc^{-1}
	$B = -13.89$ km s^{-1} kpc^{-1}

The selected values of the parameters are all listed in Table 1.

4.2. Global potential model parameters

We cannot adopt the values listed in Table 1 directly for the global potential model. The reason is that we need additional parameters to describe the global potential model, for example, the masses of the different components (bulge, disk and halo) that contribute to the potential. The values of these additional parameters are determined from the best global fit to the Galaxy according to certain observational constraints. Values of these additional parameters can be found in the literature, but if we adopt them we should also adopt the values of the other model parameters derived from the same fit. Otherwise, our model would not be internally consistent.

By adopting a set of parameters for the global potential model from the literature we demand, however, that their values be in reasonable agreement with those listed in Table 1. We adopt the parameters derived by Dauphole & Colin (1995) for a global potential model, which fulfill the above requirement. Their model consists of an axisymmetric galactic potential generated by the contributions of a spherical central bulge, a disk and an extended spherical halo. The values of the parameters were derived by Dauphole & Colin from the classical observational constraints (rotation curve, local perpendicular force, local density and Oort constants), but in addition these authors also used the dynamics of the galactic globular clusters as a constraint on the model parameters.

The values derived by Dauphole & Colin are listed in Table 2. The Sun's galactocentric distance $R_\odot$ and local circular velocity $\Theta_\odot$, as adopted by Dauphole & Colin, are $R_\odot = 8.0$ kpc and $\Theta_\odot = 225$ km s^{-1}, respectively. The total mass of the Galaxy derived from this model is 7.9×10^{11} $M_\odot$. For the Sun's motion we adopt the velocity components (9.3, 11.2, 7.6) km s^{-1}, and for the Sun's height above the galactic midplane we adopt the value $z_\odot = 10$ pc, as discussed above.

4.3. Spiral arm parameters

There is not a single, accepted picture of the global spiral structure of the Galaxy. Models differ in the number of spiral arms, m, the value of the pitch angle, γ, of the arms, and the value of the pattern speed of rotation $\Omega_{\rm p}$. Proposed global fits to observations of the Galaxy include either two or four arms, with pitch angles ranging from $\sim 5^{\rm o}$ to $\sim 27^{\rm o}$ (see Elmegreen 1985 for a review and references to these observations). For instance, Henderson (1977) and Blitz et al. (1983) obtained a four-armed pattern from HI and CO data, whereas Simonson (1976) obtained a two-armed inner structure with two additional outer arms. The use of the density-wave theory of spiral arms obtains two-armed spirals for the study of young objects in the solar neighborhood. From optical HII regions, Georgelin & Georgelin (1976) delineated four arm segments, though Bash (1981) showed that a two-armed model could also account for the HII regions used by Georgelin & Georgelin. With regard to the spiral pattern speed, results from several studies basically cluster around two different ranges of values, $\Omega_{\rm p} \simeq 11{-}14$ km s^{-1} kpc^{-1} (Lin et al. 1969; Yuan 1969a,b; Gordon 1978) and $\Omega_{\rm p} \simeq 20{-}28$ km s^{-1} kpc^{-1} (Crézé & Mennessier 1973; Nelson & Matsuda 1977; Avedisova 1989; Amaral & Lépine 1997; Mishurov & Zenina 1999). The differences between these values depends mainly on the techniques used to estimate the pattern speed. Models implying that the spiral waves travel outwards from the center of the Galaxy result in larger values of $\Omega_{\rm p}$, whereas those implying the opposite propagation direction obtain lower pattern speed values.

According to the density-wave theory of the galactic spiral arms, the density wave pattern propagates around the Galaxy with a pattern speed $\Omega_{\rm p}$ that can only extend over the part of the galactic disk for which (Lin et al. 1969)

$$\Omega - \frac{\kappa}{m} < \Omega_{\rm p} < \Omega + \frac{\kappa}{m} \tag{24}$$

where Ω is the angular velocity of rotation at a distance R, κ is the epicyclic frequency at this distance, and m is the number of spiral arms. The epicyclic frequency is defined as

$$\kappa^2 = 4\Omega^2 \left(1 + \frac{R}{2\Omega}\frac{{\rm d}\Omega}{{\rm d}R}\right). \tag{25}$$

The values of $\Omega - \kappa/m$ and $\Omega + \kappa/m$ are the inner and outer Lindblad resonances, respectively. At resonance locations, energy is dissipated and can lead to damping of spiral waves. In addition, a corotation resonance can occur if $\Omega_{\rm p} = \Omega$ for some value of R. At the corotation circle, the wave can be amplified through over-reflection (e.g., Lin & Bertin 1985). The density-wave theory works best at the zone between the inner Lindblad resonance and the corotation resonance.

In our model of the Galaxy we adopted the parameters by Dauphole & Colin (1995). In order to study the range of values of $\Omega_{\rm p}$ permitted by condition (24) and consistent with these parameters, we first derive the rotation curve of the Galaxy $\Omega(R)$ by means of a least-squares linear fit to the values tabulated by Dauphole & Colin (1995). From this curve we then determine the allowed $\Omega_{\rm p}$. The fit to the rotation curve values listed by Dauphole & Colin is

$$\left(\frac{\Omega}{\Omega_\odot}\right) = 0.965 \left(\frac{R_\odot}{R}\right) + 0.041 \tag{26}$$

where $\Omega_\odot$ and $R_\odot$ are the values listed in Table 2. Figure 3 shows the fitted curve.

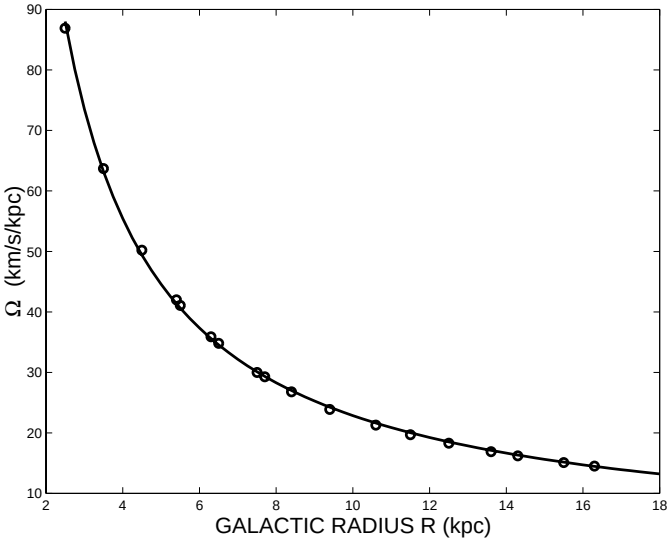

Fig. 3. Rotation curve of the Galaxy as a function of distance R from the galactic center. The circles represent the values listed by Dauphole & Colin (1995), derived from their model.

The epicyclic frequency κ as a function of distance R can be derived by introducing expression (26) and its derivative with respect to R into Eq. (25). Therefore, both $\Omega(R)$ and $\kappa(R)$ can be used to determine the range of values of the pattern speed compatible with condition (24).

We plot the rotation curve of the Galaxy Ω given by Eq. (26) in Fig. 4, and also the inner and outer Lindblad resonances (the values of $\Omega \pm \kappa/m$) for $m = 2$ and $m = 4$ spiral arms. The Lindblad resonances determine the boundary of the region where the spiral structure can exist, the region enclosed between the curves $\Omega + \kappa/m$ and $\Omega - \kappa/m$ in the plot.

For the high range of $\Omega_{\rm p}$ we consider here the two extreme values above, $\Omega_{\rm p} = 20.0$ km s^{-1} kpc^{-1} and $\Omega_{\rm p} = 28$ km s^{-1} kpc^{-1}. For the low range we consider the value of $\Omega_{\rm p} = 13.5$ km s^{-1} kpc^{-1} (Yuan 1969a). These three values are represented in Fig. 4 by the three horizontal lines. This plot suggests a preference for the two-armed over the four-armed spiral structure for low values of $\Omega_{\rm p}$. The two-armed pattern can extend over a larger region of the Galaxy. For $\Omega_{\rm p} = 13.5$ km s^{-1} kpc^{-1}, the four-armed spiral structure is limited to exist only in the outer parts of the Galaxy.

Assuming a solar galactocentric distance of $R_\odot = 8.0$ kpc, the Sagittarius arm is located at $R_{\rm a} = 6.5$ kpc, with the arm separation (distance from the Sagittarius arm to the Perseus arm) being $\Delta R \simeq 3$ kpc (Vallée 1995).

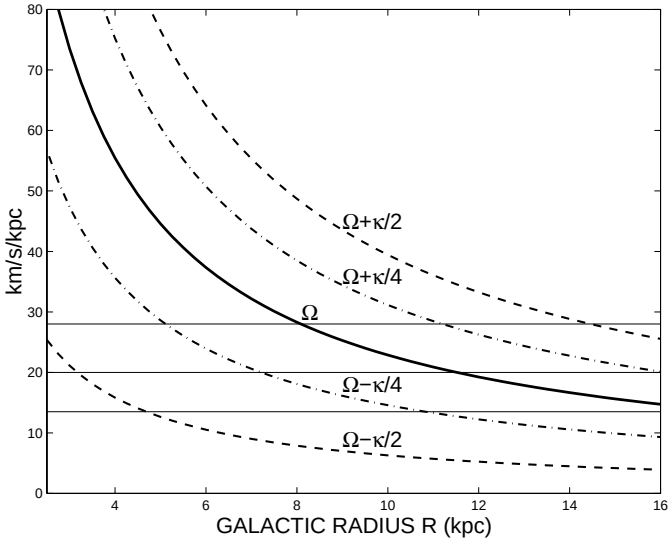

Fig. 4. Rotation curve of the Galaxy, Ω (heavy line), and $\Omega \pm \kappa/m$ curves for $m = 2$ and $m = 4$, as a function of galactic radius. The case $m = 2$ is plotted with a dashed line whereas the case $m = 4$ is plotted with a dot-dashed line. The three horizontal lines indicate where Ω_p is 13.5 km s^{-1} kpc^{-1}, 20.0 km s^{-1} kpc^{-1} and 28.0 km s^{-1} kpc^{-1}, from bottom to top, respectively.

A pure four-armed spiral structure can account for the inner galactic arms only when higher values of Ω_p are considered. From Eq. (24) we find that for the galactocentric radius $R_\odot = 8.0$ kpc the pattern speed of rotation should be $\Omega_p > 8.4$ km s^{-1} kpc^{-1} for a two-armed spiral and $\Omega_p > 18.3$ km s^{-1} kpc^{-1} for a four-armed spiral. Thus, a four-armed spiral pattern can exist in the inner galactic disk only with a pattern speed greater than $\sim$20 km s^{-1} kpc^{-1}. Moreover, in our case a four-armed structure can account for the existence of the Sagittarius arm only if pattern speeds greater than $\sim$25 km s^{-1} kpc^{-1} are considered. However, if 25.0 km s^{-1} kpc^{-1} $< \Omega_p <$ 28.0 km s^{-1} kpc^{-1}, the corotation resonance would be located at a galactic radius between that of the Perseus arm and the Sun's galactocentric distance.

Since a pure four-armed structure is constrained to a much smaller region of the Galaxy than the two-armed structure, and also to avoid corotation resonance at such a galactocentric distance, we adopt the two-armed structure for the spiral potential model. For the sake of comparison, we consider two values of the pattern speed Ω_p, 13.5 and 20.0 km s^{-1} kpc^{-1}. We list the values for the spiral potential perturbation in Table 3. We adopt the value $F = 0.05$ (Yuan 1969b) for the ratio of the radial component of the spiral field.

4.4. Choice of potential model

The local potential model assumes that for the motion of stars not far away from the galactic plane, the vertical z-force, which essentially depends on the local mass density $\rho_\odot$, can be decoupled from the R-force parallel to the galactic plane. The equation of vertical motion z results in a harmonic motion above and below the galactic midplane, which is valid only for stars with small amplitudes of oscillation, z_{max} of less than $\sim$300 pc (Binney & Tremaine 1987). For larger distances from the galactic midplane the K_z force drops below its linear value and the harmonic approximation does not work as well.

Table 3. Parameters adopted for the spiral structure of the Galaxy.

Number of spiral arms, m	2
Pitch angle, γ (degrees)	6.9°
Spiral pattern speed, Ω_p (km s^{-1} kpc^{-1})	13.5, 20.0
Ratio spiral to symmetrical field, F	0.05
Location of Sagittarius arm, R_a (kpc)	6.5
Distance Sagittarius to Perseus arm, ΔR (pc)	3.0

To estimate the validity of this approximation for our candidate stars, we calculated the amplitude z_{max} of the vertical motion of the stars for which we have radial velocity measurements, assuming a nominal value of $\rho_\odot = 0.1\ M_\odot$ pc^{-3}. Ninety per cent of the candidate stars reach a maximum distance from the galactic plane of less than 300 pc, and about one half of the stars have vertical oscillation amplitudes within 100 pc of the plane. Only 10% of the stars reach distances greater than 300 pc from the midplane, up to $\sim$1 kpc. For this 10% of stars the departure from the harmonic motion approximation may be significant. Therefore, the application of the local potential model is restricted to the case of candidate stars whose orbits are relatively close to the midplane. However, when the coupling between vertical and radial galactic forces can be neglected, this model provides a good description of the galactic potential in the solar neighborhood. It also has the advantage of allowing the use of well determined local parameters, so we can easily test the effect of varying any of these parameters on the stellar orbits.

On the other hand, dynamical mass models of the Galaxy, represented in our case by the global potential model, attempt to fit the observational parameters directly related to the force field of the Galaxy. The basic fit is to the galactic rotation curve, which contains information about the radial force field in the plane at various radial distances, and to the perpendicular force as a function of vertical height. Models thus constructed provide a description of the potential throughout the Galaxy. Therefore, the global potential model is preferred to the local potential one because its validity is not restricted to any particular region of the Galaxy or to a certain fraction of our candidate stars, contrary to what happens with the local potential model.

The global potential model parameters are adjusted to optimize the agreement between the kinematic predictions and the observational constraints of the galactic features. However, this large-scale adjustment results in a smoothed potential that might not fit local irregularities. In this case, the introduction of additional contributions from other components may be required, and the

axisymmetry of the global potential model will be broken. The strongest perturbation on the smoothed potential model comes from the potential generated by the spiral arms of the Galaxy. The use of a perturbative potential together with the global potential model would thus represent an improvement in the description of the large-scale potential of the Galaxy. However, as discussed above, the determination of the global spiral structure of the Galaxy is problematic, since an accurate description of the spiral arm features is not well established, neither qualitatively nor quantitatively. We might also consider the contribution of a galactic central bar as a perturbation of the global potential. Dehnen (2000) performed numerical simulations of the velocity distribution adopting a nearly flat rotation curve and a rotating central bar, and found a signature in the velocity distribution caused by the outer Lindblad resonance of the bar. However, the values of parameters describing the central bar, found throughout the literature and based on different studies, such as the axis ratios, the orientation of the bar, and the pattern speed, are still a matter of debate (see, e.g., Gerhard 1999 for a review). Also, Asiain (1998) performed an analysis with a sample of solar neighborhood stars and showed that the perturbation of the bar on the galactic potential is much smaller than that of the spiral arms. He further showed that the effect of the bar on the galactic orbits of solar neighborhood stars can be neglected, at least within some tens of Myr from the present time. The times of closest passage determined with our integrations of galactic orbits (see next section) are relatively short, less than ∼10 Myr, a time interval for which the effect of the central bar on the star's trajectory is not significant.

We adopt the global potential model as the most reliable model to determine the stellar galactic orbits of our candidate stars. However, we will also use the local and the spiral potential models to study the limits of the model adopted.

5. Determination of stellar encounters

We computed the galactic orbital motion of the Sun and the 595 candidate stars with measured radial velocities using the global potential model. The adopted galactic parameters are those derived by the model of Dauphole & Colin (1995), listed in Table 2. The integrations were performed for a time ±100 Myr from the present time, using a fourth-order Runge-Kutta integrator. The 100 Myr interval of time is large enough to allow all our candidate stars to encounter the solar system at their closest approach distance. From the computed stellar and solar galactic orbits, we determined the parameters of the closest approach to the Sun for each candidate star.

We list the encounters with the candidate stars in Table 4, in order of increasing miss distance $D_{\rm ca}$, for those 156 stars with a miss distance within 5 pc of the Sun. The predicted passages are contained in a time interval of ±10 Myr from the present, with most of them, ∼85%, occurring within ±3 Myr. Eighty seven of the candidate stars listed are predicted to encounter the solar system in the future, compared with 69 candidate stars having their closest approach in the past. The past/future ratio is just over one sigma different than what would be expected from random statistics.

We estimated the effect of a one sigma variation in the astrometric parameters used (parallax, proper motion in right ascension and declination, and radial velocity) on the predicted encounter parameters $D_{\rm ca}$ and $T_{\rm ca}$. We neglect the uncertainties in the position coordinates since they are very small. This estimate is given in Table 4 as $\Delta D_{\rm ca}$ and $\Delta T_{\rm ca}$. The values of $\Delta D_{\rm ca}$ and $\Delta T_{\rm ca}$ were calculated as the root sum square of the changes in $D_{\rm ca}$ and $T_{\rm ca}$ due to individual one sigma increases in the parallaxes, proper motions and radial velocities of the candidate stars

$$\Delta D_{\rm ca} = \sqrt{\sum_{i=1}^{4} (\Delta D_i)^2} \tag{27}$$

$$\Delta T_{\rm ca} = \sqrt{\sum_{i=1}^{4} (\Delta T_i)^2} \tag{28}$$

where the index i denotes the four astrometric parameters used in the calculation. The radial velocities and their uncertainties are also given in Table 4. We must caution that, in some cases, the astrometric and radial velocity errors might not be a reliable estimation of the true errors because of the long-period binaries not yet recognized.

The miss distance versus time of past (negative times) or future (positive times) encounters for the 156 passages within 5 pc are shown in Fig. 5. The shaded area represents the Oort cloud with a radius of $\sim 10^5$ AU (Smoluchowski & Torbett 1984; Antonov & Latyshev 1972). The size of the data point for each star is proportional to the visual magnitude of the star at the predicted minimum distance. We note that passages at large times are dominated by stars with the largest apparent brightness at closest approach, which suggests an observational bias. Most of the stars encountering the Sun at large times from the present epoch could only have been observed by Hipparcos at present if they are intrinsically bright. We will examine this question of observational incompleteness in more detail later.

The spatial distribution of the closest approach points on the plane of the sky in galactic coordinates, for the 156 candidate stars with miss distances less than 5 pc, is shown in Fig. 6. The solar apex and antapex directions at the present time are also noted in the plot. We use different symbols to distinguish between past and future encounters. There appears to be some signs of non-randomness in the directions to the closest approach points, in particular the low density of points in some areas of the sky such as, for instance, near the solar antapex.

To estimate if there is any departure from randomness in the distribution of encounters induced by the solar motion direction, we plot the number of stars encountered within 5 pc as a function of the angle between the solar

Table 4. Predicted stellar encounters with the solar system for passages within a heliocentric distance of 5 pc. Negative times indicate passages in the past, whereas positive times indicate future passages.

HIP[a]	Name[b]	$D_{\rm ca}$[c]	$\Delta\ D_{\rm ca}$[d]	$T_{\rm ca}$[e]	$\Delta T_{\rm ca}$[f]	$v_{\rm r}$[g]	$\sigma_{v_{\rm r}}$[h]
89825	GL 710	0.337	0.177	1357.6	40.9	−13.9	0.2
85661	HD 158576	0.938	0.705	1845.8	141.0	−46.0	1.7
70890	Proxima Centauri	0.954	0.036	26.7	0.2	−21.7	1.8
71683	α Centauri A	0.973	0.020	27.8	0.1	−22.7	1.0
71681	α Centauri B	0.975	0.020	27.7	0.2	−22.7	1.0
57544	AC+79 3888	1.007	0.033	42.8	1.2	−119.0	3.7
87937	Barnard's star	1.144	0.005	9.7	0.1	−110.9	0.2
103738	HD 199995	1.254	1.014	−3753.5	239.4	17.6	0.7
100111	HD 351880	1.434	4.617	−944.7	428.1	26.1	0.3
54035	Lalande 21185	1.440	0.006	20.0	0.1	−84.8	0.2
94512	HD 179939	1.444	1.496	3733.0	411.7	−30.7	1.8
26335	GL 208	1.600	0.054	−497.9	8.5	21.9	0.2
26624	HD 37594	1.637	0.258	−1803.5	112.1	22.4	1.3
27288	GL 217.1	1.645	0.271	−1045.6	162.7	20.0	3.7
12351	GJ 1049	1.763	0.494	−609.3	166.2	26.2	10.0
25240	HD 35317	1.775	0.505	−1077.7	73.4	52.6	1.6
86963	CD−32 13298	1.782	0.256	202.6	17.4	−27.4	2.3
99483	HIP 99483	1.797	31.108	−2889.5	1040.0	25.0	0.2
75311	BD−02 3986	1.804	9.702	3926.5	1120.8	−14.3	0.3
85605	CCDM 17296+2439B	1.837	0.551	196.8	25.8	−21.1	0.2
47425	GL 358	1.875	0.241	−62.8	7.7	142.0	21.0
92403	Ross 154	1.881	0.080	151.8	2.4	−11.5	0.8
57548	Ross 128	1.911	0.026	71.1	0.3	−30.9	0.3
86961	CD−32 13297	1.929	0.371	189.0	12.8	−28.9	0.9
110893	GL 860A	1.949	0.042	88.6	0.6	−33.8	0.2
40317	HD 68814	1.950	1.324	−2345.0	264.5	34.2	0.2
23641	HD 33487	2.001	0.358	1040.2	123.9	−39.0	5.0
30067	HD 43947	2.015	0.125	−666.4	16.2	40.2	0.1
21386	HD 26367	2.019	0.276	704.4	40.5	−50.7	1.4
35550	GL 271A	2.044	1.092	1137.8	102.5	−15.3	1.5
101573	HIP 101573	2.072	8.931	−4177.0	1246.9	43.7	0.5
20359	GL 168	2.074	0.247	380.5	21.3	−78.5	0.2
16537	Epsilon Eridani	2.135	0.077	−104.8	1.0	16.8	1.1
86214	GL 682	2.140	0.488	67.4	13.1	−60.0	21.0
38228	HD 63433	2.150	0.146	1325.6	30.3	−15.9	0.2
22738	CCDM 4535−5552A	2.202	0.460	−262.2	50.2	40.1	10.0
13772	GL 120.1	2.243	0.256	−429.9	23.7	50.6	0.7
86990	GL 693	2.253	0.311	42.0	4.9	−115.0	21.0
95326	CCDM 19236−3911B	2.262	2.153	−342.9	143.7	35.6	0.4
68634	HD 122676	2.264	0.339	−305.4	43.8	83.0	13.9
13769	GL 120.1C	2.267	0.186	−503.0	19.8	49.6	0.7
77257	GL 598	2.267	0.043	165.7	1.5	−66.8	0.3
8709	WD 0148+467	2.286	0.272	−237.2	16.5	64.0	3.0
26744	HD 37574	2.290	1.429	6118.0	1707.2	−10.0	3.7
32349	Sirius	2.299	0.090	65.7	4.7	−9.4	1.5
93506	HD 176687	2.299	0.552	−1205.6	177.3	22.0	3.7
113421	HD 217107	2.300	0.274	1403.8	153.9	−13.5	1.7
40501	GJ 2066	2.334	0.314	−133.9	16.6	62.5	10.0
31626	HD 260564	2.341	0.312	−405.2	26.4	82.7	0.2
83945	GJ 3991	2.415	0.411	145.4	22.3	−45.0	10.0
5643	GL 54.1	2.429	0.205	−74.4	1.9	28.0	3.7
11559	SAO 75395	2.469	2.049	−5409.0	847.2	20.9	0.8
25001	HD 34790	2.477	1.809	4481.0	356.3	−18.7	0.7
14576	Algol	2.481	0.930	−6878.0	1068.0	4.0	0.7
103039	LP 816−60	2.482	0.114	−270.0	6.6	15.8	0.6
33275	HD 50867	2.540	0.873	3480.0	177.2	−14.4	0.2
23708	GJ 1075	2.586	0.639	366.5	87.3	−29.2	10.0

Table 4. continued.

HIP[a]	Name[b]	D_{ca}[c]	ΔD_{ca}[d]	T_{ca}[e]	ΔT_{ca}[f]	v_r[g]	σ_{v_r}[h]
1463	GL 16	2.596	0.213	1017.9	40.3	−15.1	0.4
85429	VW Oph	2.670	2.573	542.5	205.3	−90.0	5.0
97649	GL 768	2.702	0.059	139.5	1.8	−26.1	0.7
107528	HD 207164	2.720	2.989	9565.0	674.3	−7.2	0.4
116727	GL 903	2.791	0.059	300.1	4.8	−43.1	0.7
91726	HD 172748	2.801	0.381	1248.8	72.1	−44.8	1.8
6379	GL 56.5	2.825	0.210	703.9	49.0	−22.7	1.8
82977	HD 152912	2.860	4.605	−2726.0	585.5	50.0	1.8
117473	GL 908	2.886	0.045	62.9	0.3	−71.2	0.1
116250	HD 221420	2.917	0.328	−1182.4	121.6	26.0	3.0
30920	Ross 614	2.929	0.049	−110.9	0.4	17.9	0.2
39986	HD 67852	2.932	3.158	−4366.0	1073.9	26.4	7.4
35136	GJ 1095	2.969	0.068	−189.7	2.1	84.2	0.2
37766	Ross 882	3.053	0.084	−160.4	1.4	26.6	0.2
81935	HD 150689	3.145	0.097	701.7	10.7	−19.1	0.2
20917	GL 169	3.189	0.075	294.1	2.9	−35.2	0.1
36795	GL 279	3.196	0.111	−411.7	7.0	60.1	0.3
80824	GL 628	3.208	0.038	86.0	0.2	−21.0	0.2
86162	GL 687	3.213	0.355	78.8	1.6	−27.9	6.6
77910	HD 142500	3.247	1.164	2845.0	411.9	−25.1	3.7
29271	GL 231	3.249	0.067	−255.2	4.4	34.9	0.7
80543	HD 148317	3.268	0.877	2098.0	228.3	−37.0	3.7
8102	GL 71	3.271	0.016	42.6	0.5	−16.4	0.3
27075	HD 38382	3.271	0.251	−634.7	43.2	38.7	2.8
1242	GL 1005	3.289	1.148	105.8	22.6	−29.0	21.0
3829	Van Maanen's star	3.327	0.135	−34.3	0.2	54.0	3.0
91438	GL 722	3.384	0.206	−306.6	16.6	38.6	2.5
23913	HD 233081	3.412	0.663	1842.5	123.3	−27.0	0.3
37279	GL 280A	3.438	0.035	29.6	6.9	−3.9	1.0
1475	GL 15A	3.467	0.015	−16.2	0.3	12.0	0.2
85667	GL 678	3.503	0.158	200.9	4.3	−76.4	0.5
91772	GL 725B	3.515	0.061	−0.4	0.2	0.2	0.1
33909	HD 53253	3.527	1.261	−3907.0	298.5	31.1	1.5
90112	HD 168769	3.540	1.004	−1888.0	148.4	26.0	0.3
39757	HD 67523	3.563	0.103	−394.0	7.4	46.1	0.7
91768	GL 725A	3.568	0.032	−0.4	0.2	0.2	0.1
7751	GL 66	3.569	0.118	−283.5	6.0	22.7	0.7
36208	Luyten's star	3.666	0.021	−13.9	0.1	18.2	0.1
21158	HD 28676	3.681	1.187	−5597.0	231.9	6.8	0.2
6003	HD 7735	3.692	1.599	−2219.0	749.6	31.0	15.5
105090	GL 825	3.696	0.025	−19.6	0.5	24.2	0.9
99701	GL 784	3.727	0.070	124.7	0.8	−31.1	0.7
11048	GL 96	3.756	0.113	279.9	4.0	−37.5	0.3
98698	GL 775	3.756	0.229	372.5	19.3	−31.6	2.0
25578	GL 203	3.780	0.507	−103.0	9.6	66.9	10.0
33226	GL 251	3.813	0.062	−123.9	0.3	22.7	0.2
49908	GL 380	3.856	0.021	68.7	0.1	−25.9	0.1
68184	HD 122064	3.868	0.224	333.2	16.1	−25.3	1.8
33277	GL 252	3.869	0.262	1028.6	58.1	−15.6	1.0
117748	BD+37 4901C	3.940	6.850	−4367.0	1214.3	7.4	0.7
30422	HD 44770	3.964	2.432	−1421.6	305.1	16.3	1.8
99859	HD 192869	3.979	1.650	3889.5	537.0	−28.0	3.7
101027	GL 791.1A	4.021	0.709	−1578.0	260.1	18.4	3.7
87777	HD 163547	4.056	1.373	3344.0	314.0	−43.6	1.8
34603	GL 268	4.066	0.137	−97.0	0.5	37.9	0.5
24502	HD 33959C	4.092	5.367	1828.8	739.3	−13.1	3.0
45333	GL 337.1	4.117	0.183	1285.2	43.2	−14.2	0.5

Table 4. continued.

HIP[a]	Name[b]	$D_{\rm ca}$[c]	$\Delta D_{\rm ca}$[d]	$T_{\rm ca}$[e]	$\Delta T_{\rm ca}$[f]	$v_{\rm r}$[g]	$\sigma_{v_{\rm r}}$[h]
75686	GL 585.1	4.132	0.358	589.1	25.3	−41.4	0.7
85523	GL 674	4.134	0.334	73.7	16.1	−10.2	4.5
89959	HD 168956	4.134	1.154	2831.0	404.8	−25.3	3.7
80337	GL 620.1A	4.153	0.100	−867.6	9.4	13.0	0.1
11964	GL 103	4.180	0.088	−233.2	2.6	41.9	0.5
109555	GL 851	4.205	0.145	188.3	2.6	−51.4	0.3
90595	HD 170296	4.256	1.194	2128.5	238.9	−41.0	3.7
80300	GL 620.1B	4.259	0.270	−857.6	21.8	13.0	0.1
103659	HD 199881	4.355	2.343	4874.0	392.3	−15.8	0.6
27913	GL 222	4.380	0.075	471.8	2.9	−13.4	0.1
79667	HD 146214	4.394	2.644	4807.0	636.2	−18.9	2.1
52341	GJ 1136A	4.399	1.131	−473.6	106.1	31.3	10.0
94761	GL 752A	4.420	0.055	−70.4	0.2	35.4	0.4
87345	HD 162102	4.430	2.444	3610.5	589.8	−17.5	1.8
86400	GL 688	4.461	0.167	−381.4	9.2	22.7	0.8
36186	HD 58954	4.467	1.188	2869.5	270.5	−29.2	1.8
90790	GL 716	4.484	0.119	274.7	4.3	−41.6	0.7
23452	HD 32450	4.488	0.143	351.3	4.8	−17.1	0.4
7981	GL 68	4.572	0.080	134.6	0.9	−33.9	0.7
86057	GL 680	4.573	0.771	183.9	24.0	−40.6	10.0
41820	HD 71974	4.639	0.474	1692.8	63.6	−16.1	0.2
113020	GL 876	4.690	0.046	12.1	0.7	−1.8	0.1
27693	HD 39655	4.694	1.526	−3392.0	351.6	29.3	2.5
88601	GL 702	4.698	0.117	75.2	7.6	−9.7	1.5
22449	GL 178	4.701	0.193	−211.3	4.2	24.4	1.5
88574	GL 701	4.720	0.101	−150.6	0.9	32.1	0.6
42049	HD 72617	4.760	0.756	−1063.6	134.4	53.0	7.1
86374	HD 160295	4.788	1.657	2912.0	294.6	−41.9	0.9
67529	HD 120702	4.820	0.953	2111.5	162.2	−44.0	1.8
47878	HD 84566	4.827	4.300	−6801.0	950.2	21.9	0.5
106440	GL 832	4.828	0.201	−51.5	30.5	4.1	3.0
82003	GL 638	4.834	0.073	230.1	1.0	−31.4	0.1
89937	GL 713	4.838	0.033	−155.5	0.2	32.4	0.1
114059	HD 218200	4.856	2.026	−3975.0	574.9	18.0	2.7
43670	HD 75935	4.857	0.931	2060.5	107.6	−18.9	0.3
110294	HD 239927	4.862	0.899	1569.8	161.1	−35.5	3.0
80459	GL 625	4.896	0.070	220.6	0.8	−13.0	0.3
44333	HD 77173	4.917	5.079	4909.0	887.0	−31.0	2.9
39780	HD 67228	4.924	0.239	598.8	16.9	−36.4	0.8
92871	GL 735	4.926	0.294	688.1	25.9	−13.5	0.7
53985	GL 410	4.973	0.230	529.6	16.1	−17.6	0.8
82817	GL 644	4.982	0.179	−73.6	3.3	18.8	1.8

[a] Hipparcos Catalogue number. [b] Alternative identification. [c] Distance at closest approach in pc. [d] Uncertainty in the distance at closest approach in pc; see text for details of its calculation. [e] Time of closest approach in 10^3 yr. Positive times denote close approaches in the future; negative times in the past. [f] Uncertainty in the time of closest approach in 10^3 yr; see text for details of its calculation. [g] Radial velocity in km s^{-1}. [h] Uncertainty in radial velocity in km s^{-1}.

apex at the time of the closest approach and the star's position on the plane of the sky at that time in Fig. 7. The angular bins considered are each 20° in width. We find that the number of encounters within 90° of the solar apex direction, 77, is practically the same as within 90° of the antapex, which is 79. The distribution can be fitted reasonably well by a sine curve, which is what would be expected for a random distribution, except for two angular intervals. These intervals are centered, respectively, at 90°, which shows an excess of encounters with respect to a sinusoidal distribution, and 170° (the solar antapex), which shows a deficit.

In order to assess how significant is the departure from randomness, we divide the sky into eight equal-area sections and estimate if the number of encounters in each section agrees with a random distribution. The sections are symmetric with respect to the apex-antapex direction, and correspond to the following angle intervals counted

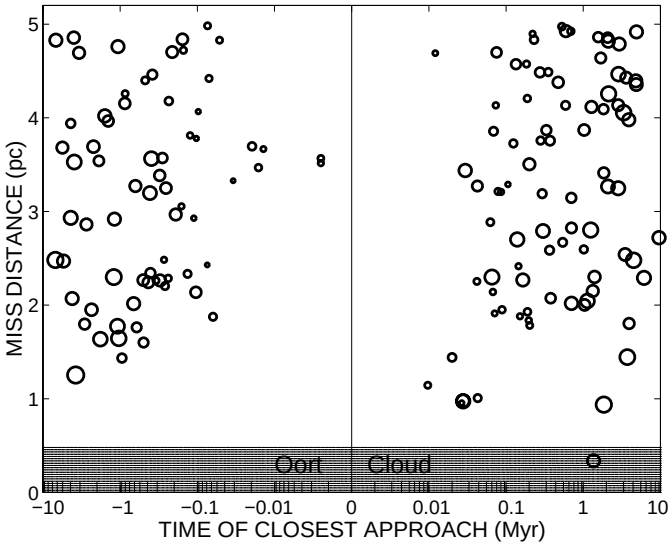

Fig. 5. Miss distance (pc) versus time (Myr) of predicted stellar approaches within 5 pc. The outer radius of the Oort cloud is approximately 10^5 AU. The circle in the shaded area denotes the predicted future passage of GL 710 through the outer Oort cloud. The size of each circle is proportional to the star's visual brightness at closest approach (stars with bigger circles are brighter). These visual magnitudes range between −4 and 12.

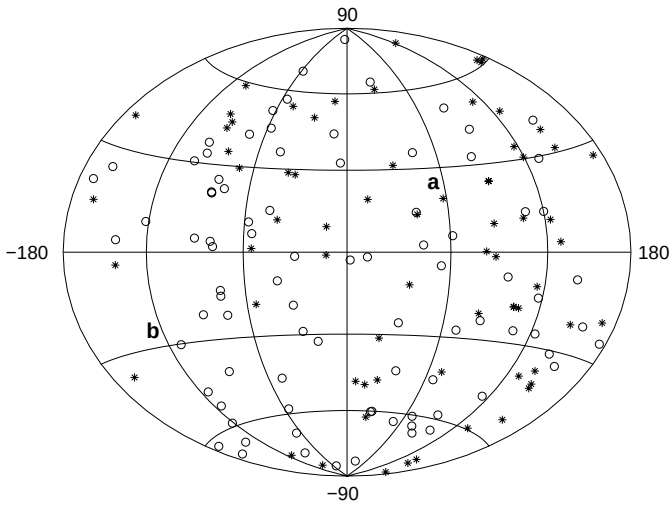

Fig. 6. Distribution of closest approach points on the plane of the sky as a function of the galactic longitude $-180° \leq l \leq 180°$ and latitude $-90° \leq b \leq 90°$. The symbol "a" denotes the solar apex and "b" the solar antapex directions. Encounters in the past are denoted by an asterisk, whereas encounters in the future are denoted by a circle.

from the solar apex direction: (0°, 41.4°), (41.4°, 60°), (60°, 75.5°), (75.5°, 90°), (90°, 104.5°), (104.5°, 120°), (120°, 138.6°), and (138.6°, 180°). If $N = 156$ is the total number of encounters within 5 pc and $s = 8$ is the number of sections, then the mean number of encounters in each section is the ratio N/s, or $\lambda = 19.5$. Assuming a Poisson distribution, the standard deviation is $\sigma = \lambda^{1/2} = 4.4$. The departure from randomness is not significant if the difference between the number of encounters in each

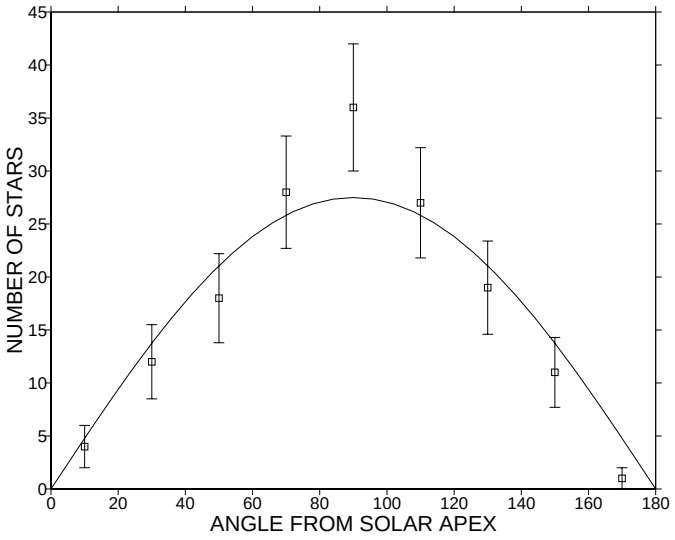

Fig. 7. Number of encounters within 5 pc as a function of the angle (in degrees) between the solar apex and the star position on the plane of the sky at the time of closest approach. The values are taken in bins of ±10°. The error bars plotted are $\pm\sqrt{n}$, where n is the value of the data point. The continuous line represents a sinusoidal distribution.

Table 5. Number of encounters in each section and deviation from the mean.

Angular interval	Number of encounters	$\mid$ Value $-\ \lambda \mid^a$
(0°, 41.4°)	17	0.6 σ
(41.4°, 60°)	17	0.6 σ
(60°, 75.5°)	22	0.6 σ
(75.5°, 90°)	21	0.3 σ
(90°, 104.5°)	26	1.5 σ
(104.5°, 120°)	22	0.6 σ
(120°, 138.6°)	19	0.1 σ
(138.6°, 180°)	12	1.7 σ

[a] Difference between the value in Col. 2 and $\lambda = 19.5$ in units of sigma.

equal-area section and the expected number of encounters λ is small. We list the number of encounters in each section as well as their difference with respect to λ in Table 5. We find that the difference is larger than one sigma in two sections. For the interval (90°, 104.5°) the number of encounters is 1.5 σ above the expected mean value, and for (138.6°, 180°) the number of encounters is 1.7 σ below the expected mean value.

Although the values in these two sections might give some evidence of non-randomness, the departure from a random distribution is not significant. Since $\lambda = 19.5$ is large, the Poisson distribution can be well approximatted by a Gaussian distribution with $\sigma = \lambda^{1/2} = 4.4$. For a Gaussian distribution, 68.27% of the cases are expected to lie within 1-σ, 86.64% within 1.5-σ, and 95.45% within 2-σ. We find that 75% of the cases lie within 1-σ, 87.5% within 1.5-σ, and 100% within 2-σ (see Table 5), which shows that the distribution is essentially Gaussian.

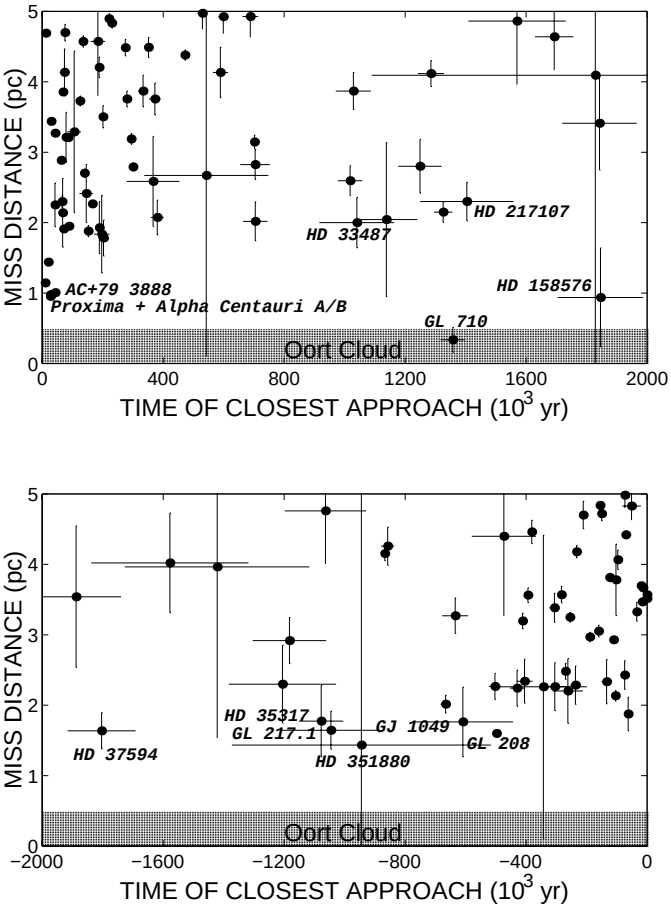

Fig. 8. Predicted stellar encounters with the Sun within 5 pc, 2 Myr in the future (top) and 2 Myr in the past (bottom). The error bars are $\pm\Delta D_{\rm ca}$ and $\pm\Delta T_{\rm ca}$, as given by Eq. (27) and (28). Names of several of the stars are noted.

The Sun's velocity relative to the LSR is about half the typical value of a star of its type, and smaller than typical velocities of most of the stellar types encountered, so in general the effect of the solar motion direction on the distribution of encounters on the sky is expected not to be significant. Nevertheless, all the values around 90° of the solar direction in Table 5 are above the mean number of encounters, whereas all the values around the solar apex or antapex direction are below the mean, which might indicate some effect of the solar motion direction. However, as seen above, this possibility is not statistically significant.

Figure 8 shows plots of the past and future stellar passages, respectively, within a time interval of ±2 Myr from the present time. The shaded area at the bottom of each plot represents the Oort cloud. Error bars given by $\pm\Delta D_{\rm ca}$ and $\pm\Delta T_{\rm ca}$ are shown. The size of some error bars is smaller than the dot size. Most of the encounters are at times close to the present time. As the time of encounter increases the number of encounters decreases. This is further evidence of the observational incompleteness mentioned above. For some stars the uncertainty in the predicted passage is very large, so the predicted encounter parameters should be considered with caution.

Table 6. Time of closest approach $T_{\rm ca}$ (in 10^3 yr) and miss distance (in pc) of GL 710 determined using different models.

Local potential model	1357.6 ± 40.9	0.337 ± 0.177
Global potential model	1357.6 ± 40.9	0.337 ± 0.177
Spiral perturbation model	1358.0 ± 40.9	0.334 ± 0.177

We find that the candidate star with the closest approach to the solar system is GL 710 (HIP 89825), a KV star with a predicted minimum distance of 0.337±0.177 pc in 1.36±0.04 Myr. This confirms our result in Paper I that GL 710 will have a passage through the outer Oort cloud, where we concluded that the perturbation caused by this passage is not strong enough to disrupt the cometary cloud. A close passage by this star was first predicted by Vyssotsky (1946) based on its low proper motion. This star is the only one of our candidate stars with a miss distance less than 10^5 AU (∼0.5 pc). In Table 6 we compare the results for GL 710 with those obtained using the other galactic potential models described above, assuming the same values of the galactic parameters. These results show that the predicted encounter with GL 710 is essentially independent of the model adopted. For the spiral perturbation model we use the two-armed configuration with two different values of the pattern speed of rotation of the spiral arms, $\Omega_{\rm p} = 13.5$ and 20.0 km s^{-1} kpc^{-1}. For both values of $\Omega_{\rm p}$ we obtain the same encounter parameters. We find an excellent agreement between the local and global potential models for the encounter with GL 710. For the calculation of the encounter parameters we assume that GL 710 is a single star. In Paper I we discussed the possible binary nature of GL 710, suspected because of the larger values of the radial velocity measurements made more than 50 years ago. We concluded that the difference in radial velocity may be due to a systematic error in the zero point of the measurements made in the 1940's. However, we also cautioned that additional monitoring of the radial velocity and the astrometric positions over the coming years is desirable to settle this conclusion.

The second closest passage is that of HD 158576 (HIP 85661), an F0 star with a predicted miss distance of 0.938 pc in 1.85 Myr. The third closest predicted approach is for the M5.5 dwarf Proxima Centauri (HIP 70890), currently the nearest star to the Sun, for which the predicted closest passage is 0.954 pc in 26 700 yr. All of the above passages are predicted for the future. The closest passage in the past was that of the G8III star HD 199995 (HIP 103738), with a predicted miss distance of 1.254 pc and time of closest approach of 3.8 Myr in the past. Eleven stars in Table 4 have errors $\Delta D_{\rm ca}$ that are larger than their predicted closest approach distances $D_{\rm ca}$. These are stars for which improved data would be particularly useful.

The closest passage of a star with an extrasolar planet candidate was that of Epsilon Eridani (HIP 16537). This K2 V star, recently proposed as a candidate for having a Jupiter-like companion of mass $M \sin i = 0.86\ M_{\rm Jup}$

(Hatzes et al. 2000), passed at a distance of 2.14 pc about 0.105 Myr ago. Encounters within 5 pc with other candidates for extrasolar planets are also predicted. HD 217107 (HIP 113421), a G7 V star with a planetary companion of mass $M \sin i = 1.27\ M_{\rm Jup}$ (Fischer et al. 1999), presently located at 19.7 pc, will pass at a heliocentric distance of 2.3 pc in 1.4 Myr in the future. GL 876 (HIP 113020), an M4 dwarf star located at 4.702 pc with a planetary companion of mass $M \sin i \simeq 2.0 M_{\rm Jup}$ (Delfosse et al. 1998), will pass at a distance of 4.69 pc in about 12 100 yr.

6. Comparison between potential models

Once we have determined the encounter parameters (miss distance and time of closest approach) for the candidate stars with the solar system using the global potential model, we are interested in studying the limits of validity of the predictions by this potential model by comparing with the other two models considered. We particularly focus our attention on the candidate stars encountering the Sun within 5 pc in a time interval of ±10 Myr, which are listed in Table 4. The encounters predicted for these candidate stars will be used later to derive the frequency of encounters with the solar system.

6.1. Comparison between global potential and local potential models

We determined the stellar encounters using both global and local potential models. For the local potential model we adopted the same values of the Sun's galactocentric distance, $R_\odot = 8.0$ kpc, and the local mass density, $\rho_\odot = 0.143\ M_\odot\ {\rm pc}^{-3}$, adopted for the global potential model.

We compare the results obtained from both models in Fig. 9. The difference ΔD between the miss distances determined by the global and the local potential models, as a function of the time of closest approach $T_{\rm ca}$, for the 156 candidate stars passing within 5 pc, is shown in Fig. 9a. For these stars the agreement between the two models is very good. The maximum difference is less than 0.2 pc, and for the overwhelming majority of stars the agreement is better than 0.03 pc. For most of the closest passages (within 2 pc) the agreement is practically perfect. The local potential model predicts passages within 5 pc of the Sun for the same candidate stars as the ones predicted by the global potential model, with the sole exception of HIP 44333. The passage for this star is predicted by the local potential model to be at a distance of 5.111 pc in 4.9 Myr, slightly greater than 5 pc, as compared to the 4.917 pc in 4.9 Myr predicted by the global potential model. This star exhibits the maximum difference in the estimated miss distances ($\Delta D \sim 0.2$ pc in the plot) between the two models.

Figure 9b shows ΔD as a function of $T_{\rm ca}$ for all 595 candidate stars. We see that for stellar passages within ∼10 Myr, the local and the global potential results are in good agreement. The differences are below 0.5 pc, except for three stars for which the differences are between 0.5 pc and 1.13 pc; these differences represent less than 8% of the actual miss distances. However, for encounter times larger than about ∼10 Myr (noted in the plot by a vertical line) the model predictions begin departing for several stars, a few of them significantly. The distribution of the 595 candidate stars as a function of ΔD is shown in Fig. 9c. We use bins of different width to better show the good agreement between the models for a large number of stars. Only ∼5% of the 595 stars have ΔD larger than 0.5 pc. The fact that the models show such a good agreement for the time interval of integration of ±10 Myr will be used later to study the variation of the predicted encounters by the adoption of different galactic parameters.

We discussed above the validity of the harmonic motion of the stars above and below the galactic midplane implied by the local potential model. The harmonic approximation cannot be used reliably for stars with amplitudes of vertical motion larger than ∼300 pc from the midplane. However, for our candidate stars with amplitudes larger than 300 pc, they only reach these amplitudes long after they have encountered the Sun. The difference in the predicted encounter parameters between the local and the global potential models is very small, practically zero for all of them.

6.2. Effect of a spiral potential perturbation on the stellar orbits

We can also study the effect of the potential of the spiral arms on the stellar passages predicted by the global potential model. First we determine the encounters within the ±100 Myr time interval of integration by using the two values of the pattern speed, $\Omega_{\rm p} = 13.5$ km s^{-1} kpc^{-1} and $\Omega_{\rm p} = 20.0$ km s^{-1} kpc^{-1} discussed above. We find a very good agreement between the miss distances obtained for both values of $\Omega_{\rm p}$. For 582 of the 595 candidate stars the agreement in encounter distance is within 0.1 pc. For the other candidate stars the differences are between 0.1 and 3 pc (only two stars have a difference larger than 1 pc) but they represent less than 4% the value of the miss distance in all but one case. The only exception is HIP 112584, with a difference of ∼55% in the value of the miss distance. However, the predicted closest passage for this star is larger than 23 pc for either of the two values of $\Omega_{\rm p}$, so this disagreement does not affect the encounters within 5 pc of the Sun. This star has the lowest heliocentric velocity in our sample, less than 1 km s^{-1}. If we adopt a pattern speed of $\Omega_{\rm p} = 20.0$ km s^{-1} kpc^{-1}, we must integrate the orbit of HIP 112584 beyond the 100 Myr interval of integration to determine its encounter with the Sun. We find a much better agreement with the global potential prediction for this star when we adopt an $\Omega_{\rm p}$ of 13.5 km s^{-1} kpc^{-1}. The differences in the integrations likely result from the very low relative velocity and long integration time, allowing small differences in the potential models to grow significantly. With this sole exception of HIP 112584, we can assume that for the candidate stars

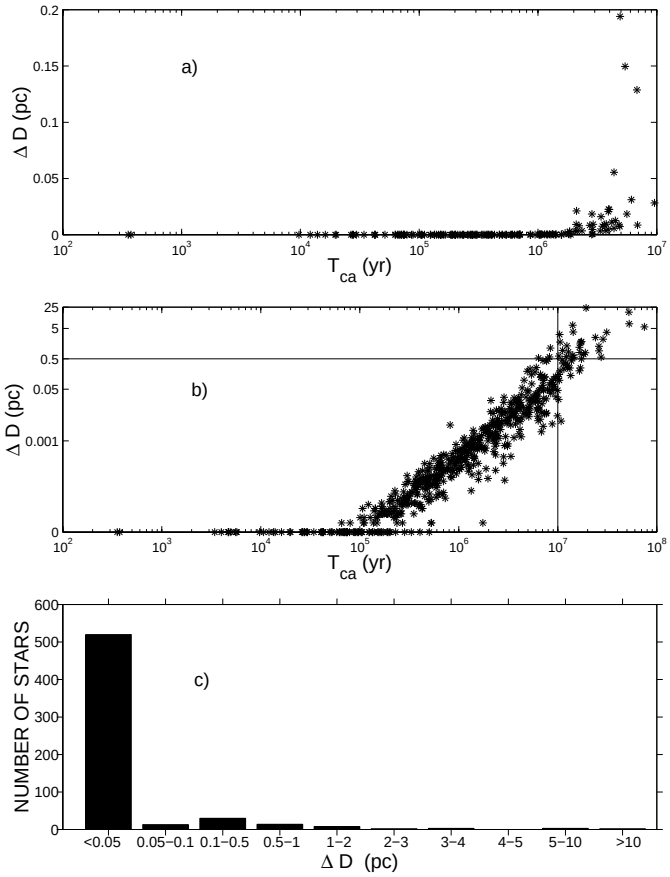

Fig. 9. a) Difference ΔD in pc between the miss distances using the global and the local potential models, as a function of time of closest approach $T_{\rm ca}$ in yr (logarithmic axis), for the 156 stars encountering the Sun within 5 pc. **b)** ΔD in pc (logarithmic axis) versus $T_{\rm ca}$ in yr (logarithmic axis) for all 595 candidate stars. Horizontal line marks $\Delta D = 0.5$ pc. Vertical line marks $T_{\rm ca} = 10$ Myr. **c)** Number of stars as a function of ΔD for the 595 candidate stars. Note that different bin widths are used.

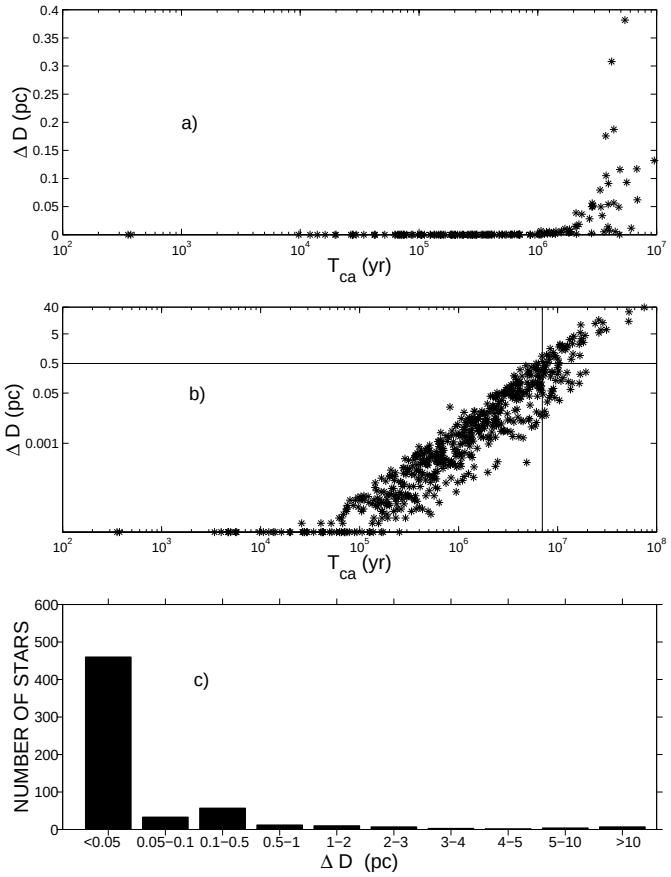

Fig. 10. a) Difference in miss distance ΔD in pc between the global potential model with and without a two-armed spiral perturbation, as a function of $T_{\rm ca}$ in yr (logarithmic axis), for the 156 stars encountering the Sun within 5 pc. **b)** ΔD in pc (logarithmic axis) versus $T_{\rm ca}$ in yr (logarithmic axis) for the 595 candidate stars. Horizontal line marks $\Delta D = 0.5$ pc. Vertical line marks $T_{\rm ca} = 7$ Myr. **c)** Number of stars as a function of ΔD for all 595 candidate stars. Note that different bin widths are used.

the spiral perturbation model predictions do not differ significantly due to the use of one or the other values of $\Omega_{\rm p}$ considered.

Figure 10a shows the difference ΔD for the global and spiral arm models as a function of time $T_{\rm ca}$ for the 156 candidate stars encountering the Sun within 5 pc, assuming a pattern speed $\Omega_{\rm p} = 13.5$ km s^{-1} kpc^{-1}. The predictions of the global potential model are not significantly affected by the spiral arms potential for most of the passages. The agreement is within 0.1 pc for most of the passages, and the maximum difference is less than 0.4 pc. Both models predict the same candidate stars passing within 5 pc of the Sun. The effect of the spiral arms on the encounters predicted within 5 pc can thus be neglected. The agreement is very good for encounters within about ± 2 Myr from the present time.

Figure 10b shows the difference ΔD as a function of time $T_{\rm ca}$ for all 595 candidate stars. We see that the effect of the spiral arms is significant for passages with large encounter times. For passages within about ± 7 Myr the difference ΔD is smaller than 0.5 pc. The vertical line in the plot denotes this time. For larger encounter times, ΔD increases roughly steadily with time for most of the passages. The distribution of the 595 candidate stars as a function of ΔD is shown in Fig. 10c. We see that, although ΔD is significant for some passages, for $\sim$92% of the 595 stars the value of ΔD is smaller than 0.5 pc.

6.3. Dependence of results on the values of the galactic parameters

We described above a range of plausible values for the parameters in the local potential model, and we also saw that the encounters predicted with the local potential model matched well those predicted by the global model. The simplicity in the use of the local potential model, where a range of values of the galactic parameters may be tested, is an advantage to predict the sensitivity of the stellar encounters to these parameters as compared with the global model. Thus, we use the local potential model, along with its plausible range of parameters, to study this sensitivity.

We tested different values of the Sun's height above the midplane, within the range $z_\odot = 0-20$ pc, and we found no significant difference in the values of the encounter parameters with respect to the ones determined using the value of $z_\odot = 10$ pc adopted for our integrations. For the extreme values of $z_\odot$ above, the average difference between the miss distances is less than 0.02%. Therefore, within this range the dependence of the encounters on the value of $z_\odot$ can be neglected.

For the distance to the galactic center we considered $R_\odot = 7.5-8.5$ kpc. We found no significant change in miss distance due to the use of values within this range. The difference is well below 0.01 pc for almost all passages. The maximum difference is 0.155 pc for HIP 79333, which is only 3% of the miss distance determined for this star. Therefore, we conclude that the effect of using values of $R_\odot$ different than 8.0 kpc within the range considered above can be neglected.

We adopted a range of $\rho_\odot \simeq 0.076-0.15\ M_\odot\ \mathrm{pc}^{-3}$ for the local mass density. As test values for this study we consider the value $\rho_\odot = 0.143\ M_\odot\ \mathrm{pc}^{-3}$ adopted for our integrations, which represents a high value of $\rho_\odot$, and the value $\rho_\odot = 0.076\ M_\odot\ \mathrm{pc}^{-3}$, which is the lower limit of the range considered. The difference ΔD between the miss distances predicted by the two values of $\rho_\odot$, as a function of the time of closest approach, is plotted in Fig. 11. The difference ΔD for the candidate stars with passages within 5 pc of the Sun is shown in Fig. 11a. The plot shows a good agreement, $\Delta D \leq 0.05$ pc, for most of the encounters. For most of the closest passages (within 2 pc) the agreement is very good. Only eight stars have 0.05 pc $< \Delta D \leq 2.2$ pc. The lower value of $\rho_\odot$ results in the addition of two passages to the list of encounters within 5 pc, whereas two other passages are removed from this list. None of the passages added or removed are within ∼4 pc or within ±3 Myr.

Figure 11b shows ΔD as a function of the time of closest approach for all 595 candidate stars. We see that the difference in the predictions for the two values of $\rho_\odot$ is significant for several encounters. The vertical line denotes a time of ±10 Myr, within which the local and the global potential model are in good agreement (see Sect. 6.1). The number of stars as a function of ΔD for encounters within ±10 Myr is plotted in Fig. 11c. Within ±10 Myr from the present time the effect of varying the local mass density $\rho_\odot$ on the stellar trajectories is a change of less than 0.05 pc in the miss distance for ∼73% of the passages. This change is larger than 0.5 pc for only ∼8% of the stars passing within ±10 Myr.

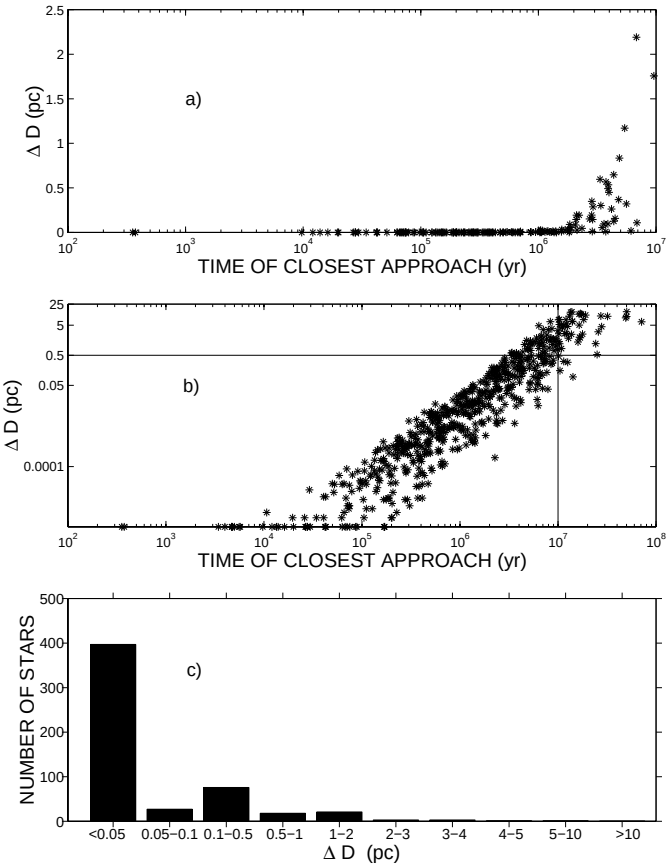

Fig. 11. a) Difference ΔD in pc between encounters predicted using $\rho_\odot = 0.076\ M_\odot\ \mathrm{pc}^{-3}$ and those using $\rho_\odot = 0.143\ M_\odot\ \mathrm{pc}^{-3}$, for the local potential model, as a function of the time of closest approach T in yr (logarithmic axis), for the 156 candidate stars encountering the Sun within 5 pc. **b)** ΔD in pc (logarithmic axis) versus T in yr (logarithmic axis) for all 595 candidate stars. Horizontal line marks $\Delta D = 0.5$ pc. Vertical line marks $T = 10$ Myr. **c)** Number of stars as a function of ΔD for encounters within ±10 Myr. Note that different bin widths are used.

6.4. Galactic parameters uncertainty versus astrometric errors comparison

We are interested in estimating the main source of uncertainty affecting our results. As sources of uncertainty we consider those arising from the values of the galactic parameters adopted for the potential model, and the observational errors on the astrometric parameters of the candidate stars.

We found that the largest changes in the predicted encounter parameters due to the galactic parameters used are for the adoption of a different value of the local mass density $\rho_\odot$, and for the contribution of the potential of the spiral arms. These two effects limit the accuracy of the stellar trajectories calculated with the global potential model. For the astrometric errors we consider the errors associated with the measured values of parallax, proper motion in right ascension, proper motion in declination and radial velocity.

To estimate whether our predictions are limited more by the potential model adopted or by the observational errors of the candidate stars, we consider ΔD_{obs} and ΔT_{obs}, the uncertainties in the prediction of the miss distance and the time of closest approach, respectively, due to the astrometric errors, and ΔD_{mod} and ΔT_{mod}, the uncertainties in the predictions of the miss distance and the time of closest

approach, respectively, due to the potential model (galactic parameters) adopted. The values of $\Delta D_{\rm obs}$ and $\Delta T_{\rm obs}$ are given by Eqs. (27) and (28). The values of $\Delta D_{\rm mod}$ and $\Delta T_{\rm mod}$ are calculated as

$$\Delta D_{\rm mod} = \mid D_{\rm ca} - D^{\star}_{\rm ca} \mid \tag{29}$$

$$\Delta T_{\rm mod} = \mid T_{\rm ca} - T^{\star}_{\rm ca} \mid \tag{30}$$

where $D_{\rm ca}$ and $T_{\rm ca}$ are the miss distance and the time of closest approach determined by the global potential model, respectively, and $D^{\star}_{\rm ca}$ and $T^{\star}_{\rm ca}$ are the miss distance and time of closest approach determined for a smaller local mass density $\rho_{\odot}$ or for the contribution of the potential of the spiral arms. The predicted encounters are constrained by the observations when $\Delta D_{\rm obs} > \Delta D_{\rm mod}$ or when $\Delta T_{\rm obs} > \Delta T_{\rm mod}$, whereas they are constrained by the potential model when $\Delta D_{\rm obs} < \Delta D_{\rm mod}$ or when $\Delta T_{\rm obs} < \Delta T_{\rm mod}$. We study the effect of each of the parameters separately.

We compare the effect of a value of $\rho_{\odot} = 0.076\ M_{\odot}\ {\rm pc}^{-3}$ on the predicted encounters with the effect of the astrometric errors. The percentage of stars with $\Delta D_{\rm obs} > \Delta D_{\rm mod}$ is ∼99% of the total number of stars. The percentage is about the same for $\Delta T_{\rm obs} > \Delta T_{\rm mod}$, ∼97%. We also compare the effect of the spiral arms of the Galaxy on the predicted encounters with the effect of the astrometric errors. We find that ∼99% of the stars have $\Delta D_{\rm obs} > \Delta D_{\rm mod}$. The percentage is the same for $\Delta T_{\rm obs} > \Delta T_{\rm mod}$. This shows that the errors in the astrometric parameters are the main effect limiting the accuracy of the predicted passages.

7. Frequency of encounters and completeness of the study

We wish to find the frequency of encounters of the Sun with star systems, where a star system is defined to contain either one or more stars. Unless we deal with a penetrating passage of a wide binary or multiple system through the Oort cloud, in which case the geometry of the system would need to be taken into account, each passage is counted as a single encounter for dynamical purposes.

The frequency of stellar passages within any distance, D, of the Sun can be estimated by

$$f = \frac{N}{t} = \pi D^2 v n_{*} \tag{31}$$

where v is the velocity of encounter of the Sun with the stellar systems and n_{*} is the local density of stellar systems (Jeans 1928; see also Weissman 1980; Hills 1981; Stern & Shull 1988). The velocity v not only depends on the Sun's peculiar velocity $v_{\odot}$, but also on the velocity dispersions of the stars encountered, v_{*}, since the stars are not at rest in space. We combine $v_{\odot}$ and v_{*} in quadrature to define the velocity of encounter, $v = \sqrt{v_{\odot}^2 + v_{*}^2}$ (e.g., Hut & Tremaine 1985). We can refine this estimate by determining the Sun's encounter frequency with different stellar types, each characterized by its own stellar velocity dispersion, density and solar motion, and adding them to obtain the total frequency of encounters. The frequency of encounters can thus be rewritten as

$$f = \frac{N}{t} = \pi D^2 \sum_i v_i n_{*i} \tag{32}$$

where index i denotes the different stellar types considered, and with relative velocity $v_i = \sqrt{v_{\odot i}^2 + v_{*i}^2}$ for each type.

For this calculation, we require the number density n_{*i} for each stellar type. This number density can be obtained from the luminosity function (LF) of star systems (the systemic LF) for the M_V interval representing each stellar type. Using data from the literature, we construct a LF as close as possible to a representative systemic LF, from which the number density can be derived.

We consider data from Gould et al. (1997) for faint stars and from Jahreiss & Wielen (1997) for main sequence stars. The values from Jahreiss & Wielen are based on data for the preparation of the new Catalogue of Nearby Stars, which also uses Hipparcos parallaxes for those catalogue stars observed by the Hipparcos satellite. This catalogue contains stars within 25 pc, and it is complete for M_V brighter than about magnitude 9 out to 25 pc. The values from Gould et al. are based on star counts for the faint end of the luminosity function. The advantage of using Gould et al.'s data is that all secondaries in binary systems are essentially missed (Frogel & Gould 1998), providing a good estimate of the systemic LF. We construct a LF based on Jahreiss & Wielen (1997) data for the interval $-1 \leq M_V \leq 9$, and on Gould et al. (1997) data for the interval $10 \leq M_V \leq 18$. This LF is listed in Table 7. From this LF we calculate the number density corresponding to the M_V interval representing each stellar type.

We also consider number densities for other stellar types. For white dwarf stars, Liebert et al. (1988) found a value of 3.2×10^{-3} pc^{-3} based on data for 43 white dwarfs contained in the Luyten Half-Second Catalogue (LHS, Luyten 1979). Leggett et al. (1998) used better measurements of the same sample, and reported a value of 3.4×10^{-3} pc^{-3}. Ruiz et al. (1993) found a factor of two larger for the number of stars observed in some areas of the sky with respect to the same areas in the LHS catalogue. This suggests a possible observational incompleteness in the LHS catalogue. Consequently, we take the Leggett et al. (1998) value and we assume it to represent a lower limit. We then correct for the fraction of these white dwarfs that are not the brightest components of binary systems, and we obtain a value of $\sim 3 \times 10^{-3}$ pc^{-3}, which we adopt as the number density of white dwarfs.

For giant stars we adopt a number density of 4.3×10^{-4} pc^{-3}, which is the difference between the general LF (for the M_V interval containing giants plus main sequence stars) and the main sequence LF reported in Jahreiss & Wielen (1997). This value is very close to the value of 4.6×10^{-4} pc^{-3} we derive from the LF

Table 7. Luminosity function $\Psi(M_V)$ adopted for the range $-1 \leq M_V \leq 18$, in units of 10^{-3} pc^{-3}.

M_V	=	−1	0	1	2	3	4	5	6	7	8	9	10	11	12	13	14
$\Psi(M_V)$	=	0.015	0.09	0.24	0.42	1.10	1.60	2.92	2.98	2.92	3.34	4.17	7.1	9.5	10.1	6.3	3.9
M_V	=	15	16	17	18												
$\Psi(M_V)$	=	1.9	1.7	2.3	2.3												

Table 8. Contribution of each stellar type to the frequency of encounters. The values of the number density n_{*i} are derived for the M_V intervals in brackets representing the stellar types, except for white dwarfs (WD) and giants.

Stellar type	M_V [a]	v_{*i} [b]	$v_{\odot i}$ [c]	n_{*i} [d]	f_i [e]
B0	(−5.7, −0.2)	14.7	18.6	0.06	0.005
A0	(−0.2, 1.3)	19.7	17.1	0.27	0.03
A5	(1.3, 2.4)	23.7	13.7	0.44	0.04
F0	(2.4, 3.6)	29.1	17.1	1.42	0.15
F5	(3.6, 4.0)	36.2	17.1	0.64	0.08
G0	(4.0, 4.7)	37.4	26.4	1.52	0.22
G5	(4.7, 5.5)	39.2	23.9	2.34	0.35
K0	(5.5, 6.4)	34.1	19.8	2.68	0.34
K5	(6.4, 8.1)	43.4	25.0	5.26	0.85
M0	(8.1, 9.9)	42.7	17.3	8.72	1.29
M5	(9.9, 18.0)	41.8	23.3	41.55	6.39
WD	–	63.4	38.3	3.00	0.72
Giants	–	41.0	21.0	0.43	0.06
Totals	–	–	–	68.33	10.525

[a] Magnitude interval. [b] Velocity dispersion in km s^{-1}. [c] Sun's peculiar velocity in km s^{-1}. [d] Number density in 10^{-3} pc^{-3}. [e] Frequency of encounters within 1 pc of the Sun per Myr.

of Scalo (1986), based also on the difference between general and main sequence LF (see also Rana 1987 for the adopted Scalo's main sequence LF). Finally, for M_V brighter than magnitude −1 we adopt a density of 8.0×10^{-6} pc^{-3} (Allen 1985). The contribution to the local density from other stellar types (e.g., supergiants, M_V brighter than −6) is not significant.

Table 8 gives the contribution of each stellar type to the frequency of encounters. Values for v_{*i} and $v_{\odot i}$ are from Mihalas & Binney (1981). From the results listed in this table we derive an expected frequency of encounters, $f_e = 10.5$ Myr^{-1} within 1 pc of the Sun. Encounters with the more massive and slow moving early-type stars are much less frequent than with the more numerous later, low mass and high velocity, types. The stellar systems that potentially may cause the greatest dynamical perturbation on the Oort cloud represent only a small fraction of all star systems. In contrast, encounters with M dwarfs represent about 73% of the total number of encounters. The contribution by white dwarfs is not very significant compared with that of M dwarfs. Even if we doubled the number density of white dwarfs, the total increase in the frequency of encounters would be less than 7%.

7.1. Frequency of encounters from the candidate stars

In order to estimate the frequency of stellar encounters with the Sun, we also considered the predicted stellar passages obtained from the global potential model integrations using the Hipparcos data, and restricted by the following times $T_{\rm ca}$ and distances $D_{\rm ca}$ of closest approach:

$$-1 \ \text{Myr} \leq T_{\rm ca} \leq 1 \ \text{Myr}; \quad D_{\rm ca} \leq 5 \ \text{pc}. \tag{33}$$

We found a total of 92 star systems in our sample encountering the Sun, which matched the criteria in (33). The mean encounter velocity of these 92 systems with the Sun is 45.7 km s^{-1} (46.7 pc Myr^{-1}). If we take this velocity as a representative value, then the star systems satisfying the conditions (33) are expected to be currently located within a heliocentric distance of ∼50 pc. In fact, we find that all 92 encounters are for star systems located within this distance.

There are 627 star systems with heliocentric distances up to 50 pc in our sample of candidate stars, from which we derived the 92 passages satisfying (33). Figure 12 is a logarithmic plot of the cumulative number of predicted encounters within 5 pc versus encounter distance, for a time interval of ±1 Myr. The dashed line in the figure is a least-squares fit to the data, which has a slope of 2.2 ± 0.2, in agreement with the theoretically predicted slope of 2. The encounters were derived from the systems with measured radial velocities, which constituted 64% of the 627 star systems. Assuming similar statistics for the total sample of 627, we find a predicted value of $f_s = 2.3 \pm 0.2$ star systems per Myr passing within 1 pc of the Sun.

7.2. Frequency of encounters corrected for observational incompleteness

The frequency of encounters derived from our candidate stars is a lower limit to the actual frequency because of the observational incompleteness in the Hipparcos data. The Hipparcos Catalogue is complete up to visual magnitude of about 7.3–9.0, depending on galactic latitude and spectral type, and has a limiting visual magnitude of ∼12. Consequently, fainter stars are missed in our study.

To correct the frequency of encounters found above, we first estimate the number of star systems within 50 pc of the Sun from the luminosity function constructed above, and then compare it with the number of star systems observed by the Hipparcos satellite. In the worst case, the Hipparcos catalogue is complete to a visual magnitude of $V_{\rm lim} \simeq 7.3$ for the entire sky, which is equivalent to a completeness to absolute magnitude $M_{V\rm lim} \simeq 4$ mag at

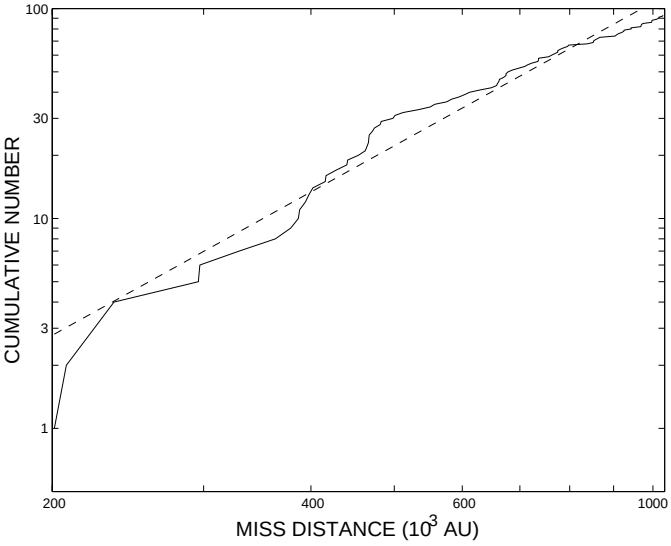

Fig. 12. Logarithmic plot of the cumulative number of predicted encounters versus miss distance $D_{\rm ca}$ (in units of 10^3 AU) The slope is 2.2 ± 0.2. The predicted encounter rate, corrected for our entire sample, is 2.3 ± 0.2 star systems per Myr passing within 1 pc of the Sun.

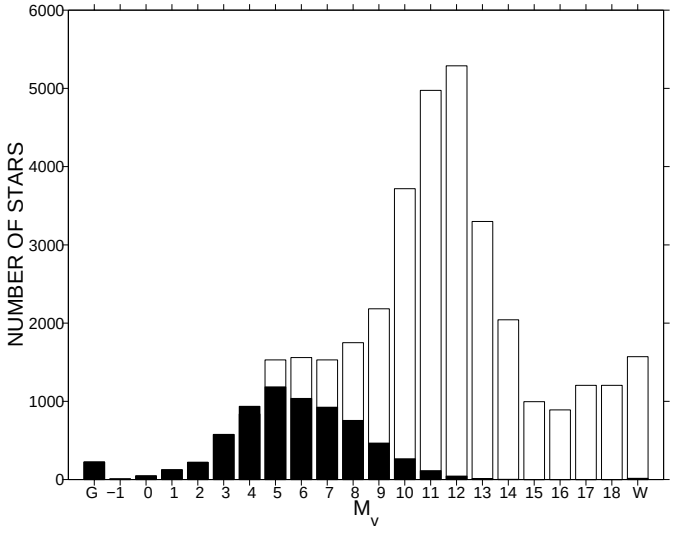

Fig. 13. Number of star systems within a heliocentric distance of 50 pc, in 1 mag bins, derived from the systemic luminosity function. The black part of each bar is the number of star systems observed by Hipparcos. The bar to the left with the label G represents giant stars, whereas the bar to the right with the label W represents white dwarfs.

a radius of 50 pc. Thus, the Hipparcos Catalogue is expected to be incomplete in this case only if M_V is fainter than ∼4.

This incompleteness is shown in Fig. 13. The plot gives the number of star systems within 50 pc estimated from the systemic LF, compared with the number detected by the Hipparcos satellite (black bar), as a function of M_V (stellar type). Main sequence stars brighter than $M_V = -1$ are not represented, since their number density (8.0×10^{-6} pc^{-3}) can be neglected.

The incompleteness of the Hipparcos data increases quickly as stars fainter than $M_V \sim 4$ are considered. Only 2% of the systems fainter than $M_V = 9$ mag are detected. Encounters with a large number of low-mass M dwarfs are, thus, missed in our sample because of the intrinsic faintness of those stars. However, encounters with M dwarfs are not likely to perturb the Oort cloud significantly because of their low masses and typically high encounter velocities, unless there is a penetrating passage through the inner comet cloud.

The number of star systems within a heliocentric radius of 50 pc predicted by the systemic LF is ∼35 800, compared with ∼7000 star systems observed by Hipparcos within this radius. Assuming statistical uncertainty in these numbers, this results in a factor $\sim 5.1 \pm 0.1$ incompleteness in the Hipparcos data. The frequency of encounters derived from our candidate stars is 2.3 ± 0.2 Myr^{-1}. To correct this value for incompleteness, we multiply by the factor 5.1 estimated above. We obtain a corrected frequency of encounters $f_{\rm c} = 11.7 \pm 1.3$ Myr^{-1} within 1 pc of the Sun. This value is in agreement within the uncertainty with the frecuency of encounters $f_{\rm e} = 10.5$ Myr^{-1} derived above from the LF.

8. Impact of future space-based astrometric missions on the search for close stellar passages

Future space-based astrometric missions are expected to provide astrometric measurements with orders of magnitude better accuracy and observe a significantly greater number of stars than Hipparcos. Moreover, these missions will observe stars that are much fainter than the Hipparcos magnitude limit. The combination of both better accuracy and a much larger number of measured stars will make it possible to improve our knowledge of the frequency of encounters with the solar system and their dynamical effect on the Oort cometary cloud.

Several space-based astrometric missions are planned to be launched in the next few years: DIVA (Double Interferometer for Visual Astrometry, launch in 2004), FAME (Full-sky Astrometric Mapping Explorer, launch in 2004), SIM (Space Interferometry Mission, launch in 2009) and GAIA (Global Astrometric Interferometer for Astrophysics, launch no later than 2012). The comparison between these missions is summarized in Table 9.

We consider two astrometric missions, GAIA and FAME, to study how future space-based missions may improve the search for close stellar passages. We choose these missions because they are expected to provide data for a larger number of stars (SIM, for instance, will observe a relatively small number of stars) and/or with better accuracy than the other astrometric missions.

8.1. The GAIA mission

GAIA, recently selected as ESA's Cornerstone 6 mission, will measure the positions and velocities of $\sim 10^9$ stars over a planned five-year mission. GAIA is the only

Table 9. Comparison between Hipparcos, SIM, DIVA, FAME and GAIA.

	Hipparcos	SIM	DIVA	FAME	GAIA
Number of objects	$\sim 1.2 \times 10^5$	$\sim 10^4$	$\sim 3.5 \times 10^7$	$\sim 4 \times 10^7$	$\sim 10^9$
Magnitude limit	$V \approx 12$	$V \approx 20$	$V \approx 16$	$V \approx 15$	$V \approx 20$
Parallax accuracy	~ 1 mas	~ 3 μas	~ 250 μas ($V = 10$)	~ 50 μas ($V = 9$)	~ 4 μas ($V = 12$)
				~ 500 μas ($V = 15$)	~ 11 μas ($V = 15$)
Proper motion acc.	~ 1 mas yr^{-1}	—	~ 400 μas yr^{-1} ($V = 10$)	~ 50 μas yr^{-1} ($V = 9$)	~ 3 μas yr^{-1} ($V = 12$)
				~ 500 μas yr^{-1} ($V = 15$)	~ 8 μas yr^{-1} ($V = 15$)
Radial velocities	No	No	No	No	Yes

space-based mission that also proposes to provide radial velocity measurements for the target stars. The radial velocity accuracy will depend mainly on spectral type, rotational velocity, and metallicity, with an accuracy of 1–10 km s^{-1} to a limiting magnitude $V \sim 17$.

To estimate how GAIA may improve the determination of stellar passages close to the Sun, we compare the uncertainty in the determination of the stellar encounters for our candidate stars due to the accuracy limits in the Hipparcos data with the uncertainty due to the expected accuracy limits of the GAIA data. We consider the 595 candidate Hipparcos stars with radial velocity measurements and we assume for these stars the errors in the parallaxes, proper motions and radial velocities expected from the measurements by GAIA. However, for those candidate stars for which we found radial velocity measurement errors in the literature smaller than the errors expected from GAIA, we adopt the errors found in the literature. All of the 595 candidate stars are brighter than visual magnitude 13. GAIA's expected accuracies for parallaxes and proper motions, 4 microarcsecond (μas) and 3 μas yr^{-1}, respectively, for $V = 12$, represent about two orders of magnitude improvement in accuracy over Hipparcos. If a given σ_i represents the actual measurement uncertainty in parallax or proper motion in the Hipparcos data, we assume that the error for GAIA is $Q\sigma_i$, where Q is the ratio between GAIA's and Hipparcos' theoretical uncertainties. Thus, the parallax uncertainty for GAIA is $0.004\sigma_i$ and the proper motion uncertainty is $0.003\sigma_i$. This implies that we assume, for instance, the same difficulties in the measurements by Hipparcos and by GAIA caused by the intrinsic physical properties of the target stars.

We define $\Delta D_{\rm G}$ as the uncertainty in the prediction of the miss distance due to the uncertainties in the parallaxes, proper motions and radial velocities (with the exceptions mentioned above for radial velocities) measured by GAIA. We also define $\Delta D_{\rm H}$ as the uncertainty in miss distance due to the uncertainties in the parallaxes and proper motions measured by Hipparcos as well as the uncertainties in the ground-based radial velocities from the literature. Both ΔD_G and $\Delta D_{\rm H}$ are calculated using Eq. (27) for the assumed uncertainties.

We plot the number of candidate stars as a function of the ratio $\Delta D_{\rm H}/\Delta D_{\rm G}$ in Fig. 14. We find that all of the predicted passages are determined with better accuracy

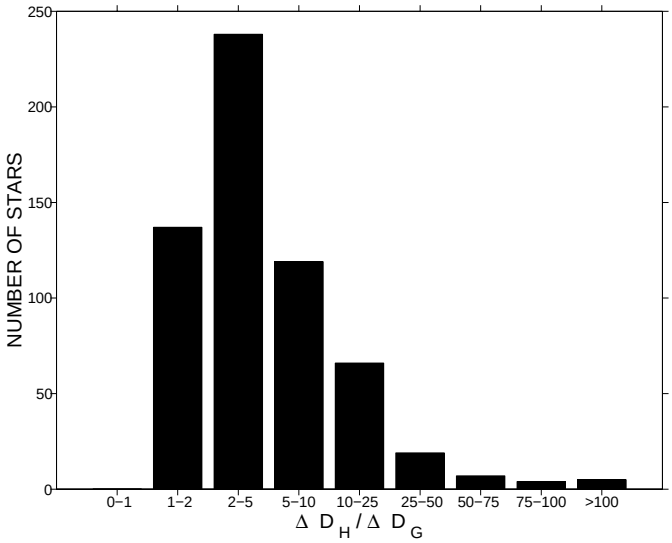

Fig. 14. Comparison between Hipparcos and GAIA in terms of the uncertainty in the determination of the closest approach distance to the Sun for the 595 candidate stars. The histogram gives the number of candidate stars as a function of the ratio between the uncertainty due to the measurement errors in the Hipparcos data and in the radial velocities, and the uncertainty due to the expected errors in the GAIA data.

assuming the uncertainty from GAIA. The error $\Delta D_{\rm G}$ is at least a factor of two smaller than the error $\Delta D_{\rm H}$ for $\sim$77% of the candidate stars. Miss distance errors are improved by more than one order of magnitude for $\sim$17% of the candidate stars (those stars with values of $\Delta D_{\rm H}/\Delta D_{\rm G} > 10$).

We also estimate the same ratio $\Delta D_{\rm H}/\Delta D_{\rm G}$ for the 595 candidate stars, but taking into account only the uncertainties in the parallaxes and proper motions, and not the uncertainties in the radial velocity measurements. We plot the number of candidate stars as a function of this ratio in Fig. 15 with the same bins as in Fig. 14. With this assumption of perfect radial velocity measurements, the predicted passages using GAIA would be determined with much better accuracy. The predicted miss distances of practically all the candidate stars are determined with an error at least a factor of two smaller than the error due to the Hipparcos uncertainty. In this case, miss distance errors are improved by more than one order of magnitude

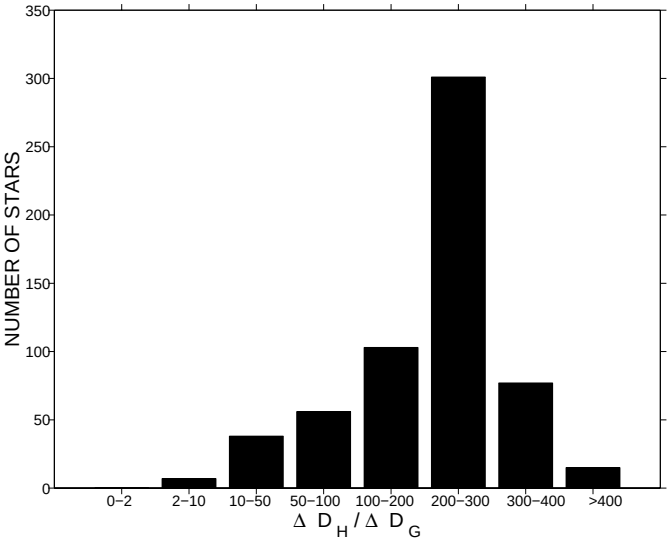

Fig. 15. Comparison between Hipparcos and GAIA in terms of the uncertainty in the determination of the closest approach distance to the Sun for the 595 candidate stars. The histogram gives the number of candidate stars as a function of the ratio between the uncertainty due to the measurement errors in the Hipparcos parallaxes and proper motions, and the uncertainty due to the expected errors in the GAIA parallaxes and proper motions. The difference with Fig. 14 is that the radial velocity measurement errors are not included here.

for ∼99% of the candidate stars, and by more than two orders of magnitude for ∼83% of the candidate stars.

From the comparison between Fig. 14, which includes the radial velocity uncertainties in the calculation, and Fig. 15, which does not include these errors, we see that the radial velocity uncertainties dominate the uncertainty in the predicted encounters over the parallax and proper motion errors. In either case, it is clear that GAIA will provide a significant improvement in the determination of close stellar encounters with the Sun, as compared with Hipparcos.

Finally, we estimate the errors in the miss distance considering the expected accuracies in parallax, proper motion and radial velocity by GAIA but, unlike above, not taking into account ground-based radial velocity measurements with better accuracy than those by GAIA. Comparing with Hipparcos results, we find that 85% of the predicted passages are determined with better accuracy assuming the uncertainty from GAIA. The errors are not improved by GAIA for the remaining 15% of the passages, though the difference is not large. The error in the determination of miss distances by GAIA is at least a factor of two smaller than the error due to the Hipparcos uncertainty for ∼65% of the candidate stars. Miss distance errors are improved by more than one order of magnitude for ∼12% of the candidate stars.

We plotted the distribution of ground-based radial velocity errors of the candidate stars in Fig. 2. About 40% of the stars in the plot have errors below 1 km s^{-1}, the best radial velocity accuracy by GAIA. Furthermore, about 16% of the candidate stars have ground-based radial velocity measurements which are between three and ten times more accurate than GAIA's value of 1 km s^{-1}. The very good accuracy of some of the ground-based radial velocities used in our study explains why GAIA, despite having better astrometric values, does not improve the uncertainty in some of the passages predicted when only the GAIA's accuracy in radial velocity is considered. It is clear that the combination of GAIA astrometric data with very accurate ground-based radial velocities provides the best results. However, such a combination will be limited to a relatively small percentage of future candidate stars, since GAIA is expected to observe a large number of stars for which no ground-based radial velocities will be available. Nevertheless, for close encounters predicted using GAIA's radial velocities, improved ground-based radial velocity data may eventually be obtained.

8.2. Frequency of encounters and completeness

We found that the observational incompleteness in the Hipparcos Catalogue is a significant source of uncertainty in the estimation of the frequency of encounters with the Sun. The future use of the GAIA data should overcome the problem of incompleteness for a large fraction of stellar types. Our estimate of the frequency of encounters was based on the star systems contained within a heliocentric distance of 50 pc. The distance modulus

$$V - M_V = 5 \log \left(\frac{d}{10} \right) \tag{34}$$

where d is the heliocentric distance of the star system (in pc), can be used to estimate the completeness of GAIA in terms of the absolute magnitude M_V. At a heliocentric distance $d = 50$ pc, the observational completeness of GAIA is given by $M_{V\lim} = V_{\lim} - 3.495$, where $V_{\lim}$ is the magnitude limit of GAIA and $M_{V\lim}$ is the absolute limiting magnitude.

Using $V_{\lim} \approx 20$ for GAIA and the equation above, GAIA will observe stars with completeness up to $M_{V\lim} \approx 16.5$ at 50 pc from the Sun. We can estimate the expected number of star systems observed by GAIA within a heliocentric distance of 50 pc, and compare it with the number of star systems observed by Hipparcos within this same distance. We consider the luminosity function adopted above and we assume that all stars or star systems brighter than $M_V = 16.5$ can be detected by GAIA within 50 pc of the Sun. For fainter stars, we calculate the distance limit within which these stars can be detected by GAIA assuming the magnitude limit of $V = 20$ for completeness. We then determine the number of stars or star systems located within this distance limit according to the luminosity function considered. The number of stars or star systems detected by GAIA is then compared with the prediction from the luminosity function.

We plot the number of stars or star systems within 50 pc of the Sun as a function of M_V (stellar type), in 1 mag bins, given by the systemic luminosity function, in Fig. 16. The plot gives the number of stars detected by

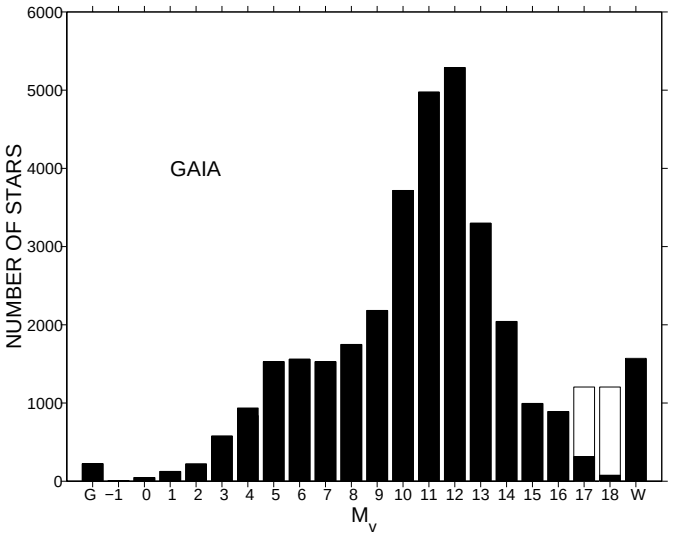

Fig. 16. GAIA completeness within 50 pc of the Sun. The plot is the same as in Fig. 13 (for the star systems observed by Hipparcos) but for GAIA.

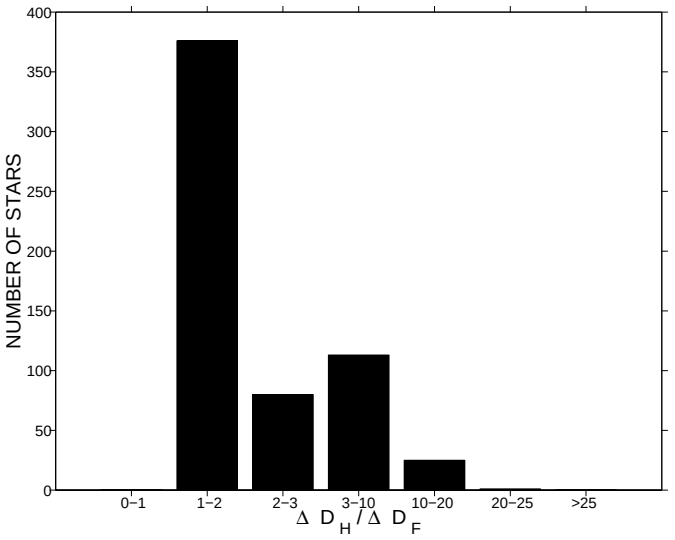

Fig. 17. Comparison between Hipparcos and FAME in terms of the uncertainty in the determination of the closest approach distance to the Sun for the 595 candidate Hipparcos stars. The histogram gives the number of candidate stars as a function of the ratio between the uncertainty due to the errors in the Hipparcos data and the uncertainty due to the expected errors in the FAME data. The errors in the ground-based radial velocity measurements are also included.

GAIA (black part of each bar). This plot can be compared with the Hipparcos completeness shown in Fig. 13. We find that GAIA should observe at least ∼95% of the star systems within 50 pc, compared with only ∼20% of star systems within 50 pc observed by Hipparcos. This represents ∼33 800 star systems observed by GAIA within 50 pc, compared with ∼7000 observed by Hipparcos within the same distance. GAIA represents a significant improvement in completeness compared with Hipparcos, which will result in a much better estimate of the frequency of stellar encounters with the Sun.

8.3. The FAME mission

FAME, a NASA MIDEX (medium-class Explorer) mission, is designed to perform an all-sky, astrometric survey that will create an accurate astrometric catalogue of 4×10^7 stars with visual magnitudes $5 < V < 15$. Unlike the GAIA mission, FAME will not measure the radial velocities of the target stars.

For FAME we proceed as in our study of GAIA, above, and consider the 595 candidate stars for which we have radial velocity measurements. For their astrometric values we assume different accuracies depending on the visual magnitude measured. For candidate stars with $V < 9$, the errors in parallax or proper motion determined by FAME are expected to be better than $0.05\sigma_i$, where σ_i represents the measurement error in parallax or proper motion in the Hipparcos data. For candidate stars with $V > 9$, the errors in parallax or proper motion determined by FAME increase, but to the limiting visual magnitude of the 595 candidate stars these errors are expected to be better than about $0.3\sigma_i$.

Adopting these uncertainties for the candidate stars, we estimate the uncertainty $\Delta D_{\rm F}$ in the prediction of the miss distances due to the expected errors in the parallaxes and proper motions measured by FAME. The uncertainty from the Hipparcos errors is $\Delta D_{\rm H}$. Both uncertainties $\Delta D_{\rm F}$ and $\Delta D_{\rm H}$ are calculated using Eq. (27). In both cases the radial velocity measurement uncertainties are those we found in the literature.

We show the number of candidate stars as a function of the ratio $\Delta D_{\rm H}/\Delta D_{\rm F}$ in Fig. 17. We find that the errors in the determination of miss distances by FAME are a factor of two or more smaller than the errors by Hipparcos for ∼37% of the candidate stars, compared with ∼77% of the candidate stars when GAIA is considered. Miss distance errors are improved by more than one order of magnitude using FAME data for ∼4% of the candidate stars, compared to ∼17% when GAIA is considered.

We also estimate $\Delta D_{\rm F}$ and $\Delta D_{\rm H}$ as above, but taking into account only the uncertainties for the parallaxes and proper motions and not the radial velocity measurement uncertainties. The number of candidate stars as a function of the ratio $\Delta D_{\rm H}/\Delta D_{\rm F}$ is shown in Fig. 18. In this case, the errors in the determination of miss distances by FAME are a factor of two or more smaller than the errors by Hipparcos for practically all the candidate stars. We also find that ∼72% of the candidate stars have one order of magnitude smaller errors with FAME, compared to ∼99% of the candidate stars with GAIA. From the comparison between Fig. 17 (with radial velocity errors) and Fig. 18 (with no radial velocity errors) we see that the radial velocity measurement uncertainties dominate the uncertainties in the predicted encounters.

FAME represents an improvement in the accuracy in the prediction of the miss distances compared to

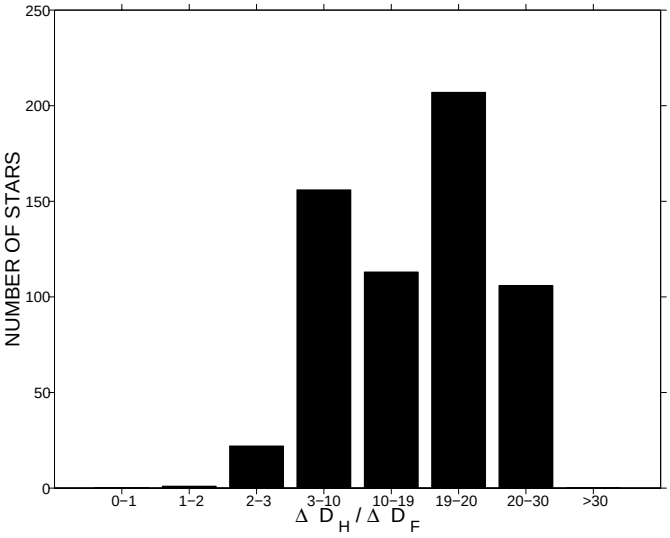

Fig. 18. Comparison between Hipparcos and FAME in terms of the uncertainty in the determination of the closest approach distance to the Sun for the 595 candidate Hipparcos stars. The histogram gives the number of candidate stars as a function of the ratio between the uncertainty due to the measurement errors in the Hipparcos data and the uncertainty due to the expected errors in the FAME data. The difference with respect to Fig. 17 is that the radial velocity measurement errors are not included here.

Hipparcos, though less than the improvement represented by GAIA. Nevertheless, FAME will play an important intermediate role since this mission should provide improved astrometric data compared to Hipparcos well in advance of GAIA. This would allow candidate stars for GAIA to be chosen, as well as radial velocity measurement programs to be initiated for candidate stars with no previous radial velocity measurements. This is especially important for long-period double and multiple systems, for which multi-epoch measurements over several years may be required to determine their systemic radial velocities.

8.4. Earth impacts and the search for close encounters

A particularly interesting aspect of the search for stars that encountered the solar system in the past is the study of possible links between records of past impact events on Earth and comet showers. It has been suggested that the terrestrial record of impacts over the last ∼250 Myr might be correlated with mass extinction events (see, e.g., Shoemaker & Wolfe 1986).

Some terrestrial impact craters have been correlated with extinction events, though crater ages are often not known well enough. However, iridium anomalies, tektites, microtektites, impact glass and shocked minerals, which constitute markers of impact events in the stratigraphic column, can be used as independent evidence to support the timing of impact events.

At least two large impact structures can be correlated with the statigraphic records in the late Eocene about 36 Myr ago, the 100-km-diameter Popigai and the 90-km-diameter Chesapeake Bay impact craters. These two craters occurred synchronously within their age uncertainty. The age of the Popigai crater is 35.7 ± 0.2 Myr (Bottomley et al. 1997), and that of the Chesapeake Bay structure is 35.5 ± 0.3 Myr to 35.2 ± 0.3 Myr (Obradovich 1989; Poag & Aubry 1995; Koeberl et al. 1996). For the last 150 Myr these combined impact craters represent the third largest known impact energy flux peak and might be correlated with global biotic crises at the end of the Eocene (Montanari et al. 1985; Montanari et al. 1998). Farley et al. (1998) found geochemical evidence for a comet shower in the late Eocene; a significant increase in the flux of extraterrestial helium-3 to Earth. Helium-3 is a tracer of fine-grained interplanetary dust. Farley et al. suggested that the correlation between increased concentrations of helium-3 and large impacts indicates that the abundance of Earth-crossing objects and the dustiness of the inner solar system were simultaneously but only briefly enhanced. The flux of extraterrestial helium-3 began to increase before the impact events, reached a maxima coincident with those impacts, and then rapidly declined.

We estimated that the time horizon for our search for encounters with the solar system using Hipparcos data is roughly about ±10 Myr from the present time. The observational incompleteness in the Hipparcos Catalogue limits the determination of stellar encounters to within a few million years, beyond which the number of close passages missed by our search is very large. In contrast, GAIA may enhance this time interval to, at least, the past several tens of million years, as suggested by the comparison between Figs. 13 and 16. This is the time period required to cover the known cratering events in the late Eocene. Thus, the GAIA mission may provide sufficiently accurate data for a remarkably large number of stars to study the possible link between comet showers and records of past impact events on Earth.

We can estimate the number of main sequence stars with masses $\geq 1\ M_\odot$ that can be detected, and their radial velocities measured, by GAIA. A close or penetrating passage of this massive a star through the Oort cloud could have caused a comet shower in the past. We adopt an absolute magnitude of $M_V = 4.8$ (which corresponds to the Sun's value and which is equivalent to a lower mass limit) or brighter for this estimate. GAIA is complete to $V \approx 20$. However, to calculate the stellar trajectories we need radial velocity data, and the limiting magnitude for radial velocity measurements is $V \sim 17$, which we adopt for the calculation.

The effect of the interstellar absorption and scattering of light, A_V, cannot be neglected because of the large distances involved. We can consider A_V to be proportional to the distance of the observed star, and assume a standard value of one magnitude per kpc for the dimming effect on the star's brightness. We consider the equation

$$V - M_V = 5 \log (d) - 5 + 0.001d \qquad (35)$$

where the distance d is given in pc and $A_V \equiv 0.001d$. Taking the values $V = 17$ and $M_V = 4.8$ above, and

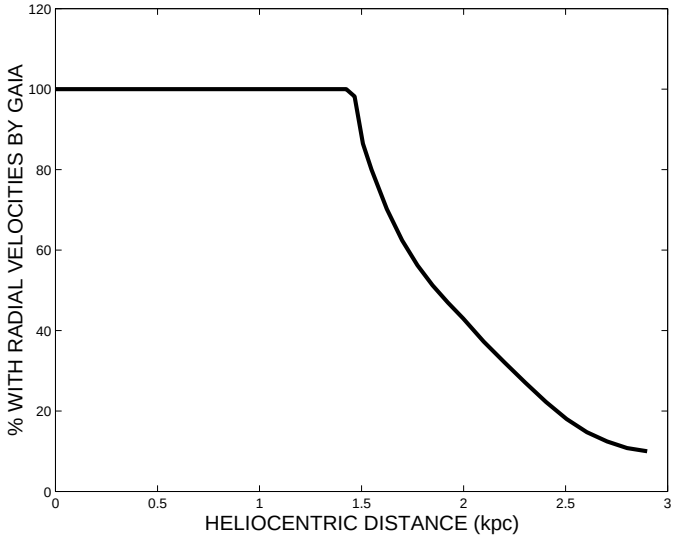

Fig. 19. Percentage of solar-type or more massive stars that will have their radial velocities measured by GAIA, as a function of the heliocentric distance in kpc. The expected completeness for GAIA stars with radial velocity measurements is to a distance of ∼1.4 kpc.

solving the equation, we find a distance of $d \simeq 1.4$ kpc. Thus, GAIA should provide astrometric and radial velocity data for all solar-type or more massive stars located within a heliocentric distance of $d \simeq 1.4$ kpc. The heliocentric distance to which GAIA's astrometry is observationally complete for solar-type or more massive stars, that is for the limiting magnitude of 20, is $d \simeq 2.9$ kpc. Between these two heliocentric distances only a percentage of these stars observed by GAIA will also have their radial velocities measured. We estimated this percentage based on the luminosity function adopted. The results are shown in Fig. 19. The number of stars with radial velocity measurements by GAIA begins to decrease for distances larger than ∼1.4 kpc, beyond which only the more massive, brighter stars will be measured.

The Hipparcos completeness for these solar-type or more massive candidate stars is to a distance of only ∼30−60 pc, according to the Hipparcos magnitude limit of 7.3−9.0. GAIA, with $d \simeq 1.4$ kpc, represents an improvement of a factor of 23−47 with respect to Hipparcos, in terms of the limit distance within which completeness for the search for these candidates can be achieved. This corresponds to an increased search volume more than 12 000 times that achieved by Hipparcos. In fact, this is a lower limit estimate since only a limited number of the Hipparcos star candidates have ground-based radial velocity measurements. The time horizon for completeness in the prediction of close passages in the past using GAIA is expected to be increased accordingly. It is difficult to estimate the typical time horizon for completeness because of the complexities of the stellar galactic orbits for the integration times involved. However, as a rough estimate, we can assume the same order of magnitude increase in the time horizon as in the increase in the distance horizon expected with the use of GAIA data. Therefore, the time horizon for the search for the candidate star that might have caused a comet shower can very likely be expanded by GAIA beyond the ∼36 Myr ago date of the late Eocene impact events. Stars with slower encounter velocities are likely to have a bigger effect on the Oort cloud. Thus, perhaps the time horizon is even longer for these stars since they will not be as far from the Sun compared to faster moving stars. Of course, the transient nature of the stars must be taken into account, since only those with lifetimes beyond the ∼36 Myr of the late Eocene events can be included in the search. Thus, massive early-type stars with short lifetimes should be ruled out. This type of stars, however, represents only a small fraction of the candidate stars.

An issue to be considered is that, with improved astrometric values, the ultimate limit on predicting close passages over the integration times required to account for the late Eocene event will be the galactic potential model, as well as the difficulty in recreating star-star and star-GMC encounters. Although it is difficult to quantify how accurately a stellar trajectory can be determined over such integration times, it seems clear that the uncertainty in the galactic parameters strongly limits the prediction capability. The largest source of error for encounters over timescales of several tens of Myr comes from the uncertainty in the density of matter in the galactic disk and the density variation, as shown above when we discussed the validity of our results. Thus, we need improved models of the Galaxy to reproduce better the actual gravitational potential if we want to predict accurately a close passage during the late Eocene event. However, better astrometric measurements can also lead to better potential models. This will improve our ability to integrate galactic orbits over longer timescales.

A more difficult problem is that of star-star and star-GMC perturbations. In Paper I we showed that such perturbations can be neglected on timescales of a few Myr. However, they may become more significant over the ∼40 Myr timescale we would like to achieve with the FAME and GAIA data. Also, the short lifetimes of massive, early-type stars, which could act as significant perturbers, may make it impossible to recreate stellar trajectories with any reliability. It is even possible that a massive, early-type star was the late Eocene perturber, and that the star no longer exists, and thus can never be found.

9. Conclusions

1. We found that 156 candidate stars have passed or will pass within 5 pc of the Sun during about ±10 Myr from the present time, with most of them, ∼85%, ocurring within a time interval of ±3 Myr. The passages at large times are dominated by stars with the largest apparent brightness at closest approach, which suggests an observational bias that we interpreted as the result of observational incompleteness in the Hipparcos data.

2. Within a time interval of about ±10 Myr from the present time, the predicted encounters are fairly well determined for most of the candidate stars. They are not altered significantly by the use of alternative galactic potential models or by varying the plausible values of the galactic parameters. It is the astrometric errors that ultimately limit the accuracy of the predicted encounters for most of our candidate stars over the time interval of integration considered. The time interval of about ±10 Myr from the present time is essentially an upper limit in our search for close stellar passages.
3. The most interesting result is the future passage of the star GL 710 through the outer Oort cloud. We determined a miss distance of 0.337 ± 0.177 pc in 1.36 ± 0.04 Myr from the present for the passage of this star. These values are in excellent agreement with the predictions using the other galactic potential models, indicating that the prediction of this passage is not model dependent.
4. We estimated a value of 10.5 star systems per million years encountering the Sun within one pc based on a luminosity function constructed from data available in the literature. About 73% of the expected encounters are with late-type, low mass M dwarfs. The frequency of encounters with the Sun was also estimated using the predicted passages for the Hipparcos candidate stars. We found a value of 2.3 ± 0.2 star systems per Myr passing within one pc of the Sun. This value represents a lower limit because of the observational incompleteness in the Hipparcos data. We corrected this value for incompleteness and derived a frequency of encounters with the Sun of 11.7 ± 1.3 star systems per Myr within a radius of one pc. Future measurements of radial velocities for the full sample of candidate stars are expected to improve the estimate of the lower limit above.
5. Based on the predicted encounters for the 595 candidate Hipparcos stars, we found that GAIA and FAME would significantly decrease the uncertainty in the determination of the stellar encounters with the Sun. Radial velocity measurement errors would represent the dominant uncertainty factor in the passages predicted using data from these proposed missions. We expect a dramatic improvement in the determination of the frequency of encounters using GAIA data due to the much greater observational completeness estimated for that mission.
6. We suggest that GAIA may provide, for the first time, sufficiently accurate data and for a large enough number of stars to carry out a reliable study of the links between comet showers and past impact events on Earth. In particular, we considered the case in which records of multiple large impacts on Earth might be correlated with a comet shower during the late Eocene, ∼36 Myr ago. GAIA should significantly increase the distance horizon that limits the search for past close encounters using Hipparcos data, and consequently expand the time horizon of our search beyond the ∼36 Myr age of the late Eocene event. However, the galactic potential models may limit the prediction capability for encounters with large integration times.

Acknowledgements. We thank the suggestions made by an anonymous referee. This research was carried out in part at the Jet Propulsion Laboratory, California Institute of Technology, under contract with the National Aeronautics and Space Administration, and was supported in part by the Planetary Geology and Geophysics Program.

References

Allen, C. W. 1985, Astrophysical Quantities, 3rd. ed. (Atholone Press, London)
Amaral, L. H., & Lépine, J. R. D. 1997, MNRAS, 286, 885
Antonov, V. A., & Latyshev, I. N. 1972, in The Motion, Evolution of Orbits and Origin of Comets, ed. G. A. Chebotarev, E. I. Kazimirchak-Polonskaya, & B. G. Marsden (Reidel, Dordrecht), 341
Asiain, R. 1998, Ph.D. Thesis, Universitat de Barcelona, Spain
Avedisova, V. S. 1989, Ap, 30, 83
Bahcall, J. N. 1984a, ApJ, 276, 169
Bahcall, J. N. 1984b, ApJ, 287, 926
Bahcall, J. N., Flynn, C., & Gould, A. 1992, ApJ, 389, 234
Bash, F. N. 1981, ApJ, 250, 551
Bertin, G., & Lin, C. C. 1996, Spiral Structure in Galaxies: A Density Wave Theory (The MIT Press, Cambridge, MA)
Bienaymé, O., Robin, A. C., & Crézé, M. 1987, A&A, 180, 94
Binney, J., & Tremaine, S. 1987, Galactic Dynamics (Princeton University Press, Princeton, NJ)
Blitz, L., Fish, M., & Kulkarni, S. 1983, Science, 220, 1233
Bottomley, R., Grieve, R., York, D., & Masaitis, V. 1997, Nature, 388, 365
Crézé, M., & Mennessier, M. O. 1973, A&A, 27, 281
Crézé, M., Chereul, E., Bienaymé, O., & Pichon, C. 1998, A&A, 329, 920
Dauphole, B., & Colin, J. 1995, A&A, 300, 117
Delfosse, X., Forveille, T., Mayor, M., et al. 1998, A&A, 338, L67
Delhaye, J. 1965, in Galactic Structure, ed. A. Blaauw & M. Schmidt (Univ. Chicago Press, Chicago), 61
Dehnen, W. 2000, AJ, 119, 800
Elmegreen, D. M. 1985, in The Milky Way Galaxy (Kluwer, Dordrecht) IAU Symp., 106, 255
The Hipparcos and Tycho Catalogues 1997, ESA SP-1200, Noordwijk
Farley, K. A., Montanari, A., Shoemaker, E. M., & Shoemaker C. S. 1998, Science, 280, 1250
Feast, M., & Whitelock, P. 1997, MNRAS, 291, 683
Fischer, D. A., Marcy, G. W., Butler, R. P., Vogt, S. S., & Apps, K. 1999, PASP, 111,50
Frogel, J. A., & Gould, A. 1998, ApJL, 499, 219
García-Sánchez, J., Preston, R. A., Jones, D. L., et al. 1997, in Proceedings of the ESA Symp. Hipparcos – Venice 97, ed. B. Battrick (ESA SP-402, Noordwijk), 617
García-Sánchez, J., Preston, R. A., Jones, D. L., et al. 1999, AJ, 117, 1042
Georgelin, Y. M., & Georgelin, Y. P. 1976, A&A, 49, 57
Gerhard, O. E. 1999, in Galaxy Dynamics, ed. D. R. Merrit, M. Valluri, & J. A. Sellwood (ASP, San Francisco), ASP Conf. Ser., 182, 307

Gordon, M. A. 1978, ApJ, 222, 100
Gould, A., Bahcall, J. N., & Flynn, C. 1997, ApJ, 482, 913
Hatzes, A. P., Cochran, W. D., McArthur, B., et al. 2000, ApJL, 544, L145
Henderson, A. P. 1977, A&A, 58, 189
Hills, J. G. 1981, AJ, 86, 1730
Holmberg, J., Flynn, C., & Lindegren, L. 1997, in Proc. of the ESA Symp., Hipparcos – Venice 97, ed. B. Battrick (ESA SP-402, Noordwijk), 721
Holmberg, J., & Flynn, C. 2000, MNRAS, 313, 209
Humphreys, R. M., & Larsen, J. A. 1995, AJ, 110, 2183
Hut, P., & Tremaine, S. 1985, AJ, 90, 1548
Hut, P., Alvarez, W., Elder, W. P., et al. 1987, Nature, 329, 118
Jahreiss, H., & Wielen, R. 1997, in Proc. of the ESA Symp., Hipparcos – Venice 97, ed. B. Battrick (ESA SP-402, Noordwijk), 675
Jeans, J. H. 1928, Astronomy and Cosmogony (Cambridge University Press, Cambridge)
Kerr, F. J., & Lynden-Bell, D. 1986, MNRAS, 221, 1023
Koeberl, C., Poag, C. W., Reimold, W. U., & Brandt, D. 1996, Science, 271, 1263
Kuijken, K., & Gilmore, G. 1989, MNRAS, 239, 651
Kuzmin, G. G. 1956, AZh, 33, 27
Latham, D. W. 1985, in Stellar Radial Velocities, ed. A. G. D. Philip, & D. W. Latham (Davis, Schenactady, N. Y.), IAU Colloq., 88, 21
Latham, D. W. 1992, in Complementary Approaches to Double and Multiple Star Research, ed. H. A. McAlister, & W. I. Hartkopf (ASP, Chelsea), ASP Conf. Ser., 32, 158
Leggett, S. K., Ruiz, M. T., & Bergeron, P. 1998, ApJ, 497, 294
Liebert, J., Dahn, C. C., & Monet, D. G. 1988, ApJ, 332, 891
Lin, C. C., Yuan, C., & Shu, F. H. 1969, ApJ, 155, 721
Lin, C. C., & Bertin, G. 1985, in The Milky Way Galaxy (Kluwer, Dordrecht), IAU Symp., 106, 513
Luyten, W. J. 1979, The LHS Catalogue, 2d ed., Univ. Minnesota, Minneapolis
Mihalas, D., & Routly, P. M. 1968, Galactic Astronomy (Freeman, San Francisco)
Mihalas, D., & Binney, J. J. 1981, Galactic Astronomy, 2nd ed. (Freeman, San Francisco)
Mishurov, Y. N., & Zenina, I. A. 1999, A&A, 341, 81
Miyamoto, M., & Nagai, R. 1975, PASJ, 27, 533
Montanari, A., Drake, R., Bice, D. M., et al. 1985, Geology, 13, 596
Montanari, A., Bagatin, A. C., & Farinella, P. 1998, Planetary and Space Science, 46, 271
Nelson, A. H., & Matsuda, T. 1977, MNRAS, 179, 663
Obradovich, J. D., Snee, L. W., & Izett, G. A. 1989, Geol. Soc. Am. Abstr. Programs, 21, 134
Olling, R. P., & Merrifield, M. R. 1998, MNRAS, 297, 943
Pham, H-A. 1997, in Proc. of the ESA Symp. Hipparcos – Venice 97, ed. B. Battrick (ESA SP-402, Noordwijk), 559
Plummer, H. C. 1911, MNRAS, 71, 460
Poag, C. W., & Aubry, M-P. 1995, Palaios, 10, 16
Rana, N. C. 1987, A&A, 184, 104
Reed, B. C. 1997, PASP, 109, 1145
Reid, M. J. 1993, ARA&A, 31, 345
Reid, M. J., Readhead, A. C. S., Vermeulen, R. C., & Treuhaft, R. N. 1999, ApJ, 524, 816
Rickman, H. 1976, Bull. Astron. Inst. Czechoslovakia, 27, 92
Ruiz, M. T., Takamiya, M. Y., Méndez, R., Maza, J., & Wishnjewsky, M. 1993, AJ, 106, 2575
Scalo, J. 1986, Fundamentals of Cosmic Physics, vol. 11
Shoemaker, E. M., & Wolfe, R. F. 1986, in The Galaxy and the Solar System, ed. R. Smoluchowski, J. N. Bahcall, & M. S. Matthews (Univ. Arizona Press, Tucson), 338
Simonson, S. C. 1976, A&A, 46, 261
Smoluchowski, R., & Torbett, M. 1984, Nature, 311, 38
Stern, S. A., & Shull, J. M. 1988, Nature, 332, 407
Trumpler, R. J., & Weaver, H. F. 1953, Statistical Astronomy (Dover, New York)
Vallée, J. P. 1995, ApJ, 454, 119
Vyssotsky, A. N. 1946, PASP, 58, 166
Weissman, P. R. 1980, Nature, 288, 242
Weissman, P. R. 1996, Earth, Moon & Planets, 72, 25
Yuan, C. 1969a, ApJ, 158, 871
Yuan, C. 1969b, ApJ, 158, 889